TWO DIMENSIONAL SPATIAL COHERENCE OF SKELETAL MUSCLE'S NATURAL VIBRATIONS DURING VOLUNTARY CONTRACTIONS.

A Thesis
Presented to
The Academic Faculty

by

Akibi A. A. Archer

In Partial Fulfillment
of the Requirements for the Degree
Master of Science in the
George W. Woodruff School of Mechanical Engineering

Georgia Institute of Technology
December 2010

TWO DIMENSIONAL SPATIAL COHERENCE OF SKELETAL MUSCLE'S NATURAL VIBRATIONS DURING VOLUNTARY CONTRACTIONS.

Approved by:

Professor Karim G. Sabra, Advisor
George W. Woodruff School of Mechanical Engineering
Georgia Institute of Technology

Professor Minoru Shinohara
School of Applied Physiology
Georgia Institute of Technology

Professor Jun Ueda
George W. Woodruff School of Mechanical Engineering
Georgia Institute of Technology

Date Approved: September 16, 2010

I would like to first give thanks to the Creator, because without the Creator none of this work would be possible. There were many people that have supported me during my studies thus far at the Georgia Institute of Technology, I will be forever grateful of their support. My research work would not have been possible without them. I would like to give thanks to my thesis committee comprising of Dr. Karim G. Sabra, Dr. Minoru Shinohara and Dr. Jun Ueda. My deepest gratitude is to my advisor, Dr. Karim G. Sabra whose knowledge and expertise guided me through the research process. I would also like to thank my lab mates for their assistance with different portions of my research project, especially Shaun Anderson and Paul Langston. A special thanks goes to Ashley N. Johnson who steadily assisted me with the progression of my research. Also to Perry Atangcho, who assisted me with collecting and analyzing much of the data for this thesis. There were other people at the Georgia Institute of Technology that made my life easier, who were not directly related to research. In that regard I would like to thank Camellia Henry, Terri Keita, Trudy Allen and Glenda Johnson. My family and friends have been a continuous support system for me throughout my academic career. I would like to thank my parents for pushing me to excel and knowing that I can. The encouragement of my family and friends kept me going through times that were challenging. To them I give them most thanks. Last but not least I would like to give thanks to my ancestors whose scientific expertise and understanding has been instilled in me necessary commitment and strength to succeed.

TABLE OF CONTENTS

LIST OF FIGURES

SUMMARY

A means for non-invasively diagnosing and monitoring muscular activity can be obtained by measuring the in-vivo viscoelastic properties of skeletal muscle (muscle stiffness). Such measurements are scarce, though skeletal muscles are essential components of human motor function. The techniques that due exist are often invasive. For instance, standard elastography techniques rely on an external mechanical or radiation excitation to generate vibrations into the skeletal muscle that can be measured to estimate their viscoelastic properties. Skeletal muscles are made up of striated fibers that attach to the skeleton via tendons and are responsible for voluntary body movements. Low frequency mechanical oscillations (<100 Hz) also called muscle noise, are naturally generated by skeletal muscles during voluntary contractions. This study will use miniature skin mounted accelerometers to measure this muscle noise. The measurement using these accelerometers are called surface mechanomyograms (S-MMGs).

This research focused on determining the directionality of the propagating S-MMG waves, also determined how these S-MMG waves vary with frequency, sensor separation distance as well as muscle contraction level. Using a 2 dimensional grid of 1 dimensional accelerometers placed on the biceps brachii muscle, these characteristics of S-MMG waves will be explored. The directionality of the S-MMG propagation will be investigated by analyzing the similarity between the recorded signal at different points on the 2-dimensional 3 $\times$ 5 grid. This similarity measure of the two recorded signals is called the spatial coherence. The spatial coherence will be used to analyze the S-MMG's dependency on frequency, sensor separation distance, muscle

contraction level and finally directionality. Similarity between sensor pairs located along the longitudinal axis of the muscle will be compared to the similarity between sensor pairs located transversely across the long axis of the muscle. This analysis will determine specific directionality with-in a specific frequency band and across all contraction levels and sensor separation distances.

CHAPTER I

INTRODUCTION

1.1 Background

1.1.1 Skeletal Muscle

In the human body, skeletal muscle is tailored for force generation and movement. Due to the relationship of structure-function of the skeletal muscle, when studying muscle function, muscle structure must also be taken into consideration. All skeletal muscles attach to connective tissue (tendons) in order to connect to the bone. The skeletal muscle architecture can be defined as the arrangement of muscle fibers relative to the axis of force generation [39]. For example, the biceps brachii has muscle fibers that extended parallel to the axis of force generation and are termed longitudinal or parallel muscle. The human muscles contain a mixture of muscle fiber types and motor units. Heterogeneous muscle contain slow contracting (high endurance) and fast contracting (low endurance) fibers. At the proximal end the biceps brachii has two distinct muscle fiber groups; the short head which originates at the tip of the coracoid process and the long head which originates at the supraglenoid tubercle. Both heads of the muscle join together and have an insertion point at the radial tuberosity (see Fig. 1). The biceps brachii (at least in its lower section) is fusiform with almost parallel muscle fibers (see Fig. 1) [29]. The specific tendons that drive the elbow flexion mechanism attaching the biceps to the skeleton differ at the extremities. The origin tendons of both bicep heads attach separately to the relatively fixed bone of the articulation (at the shoulder scapula). The insertion tendon is attached to the moving part of the articulation (at the humerus) (Fig. 1).

In basic physiological terms an isometric contraction is a contraction where the

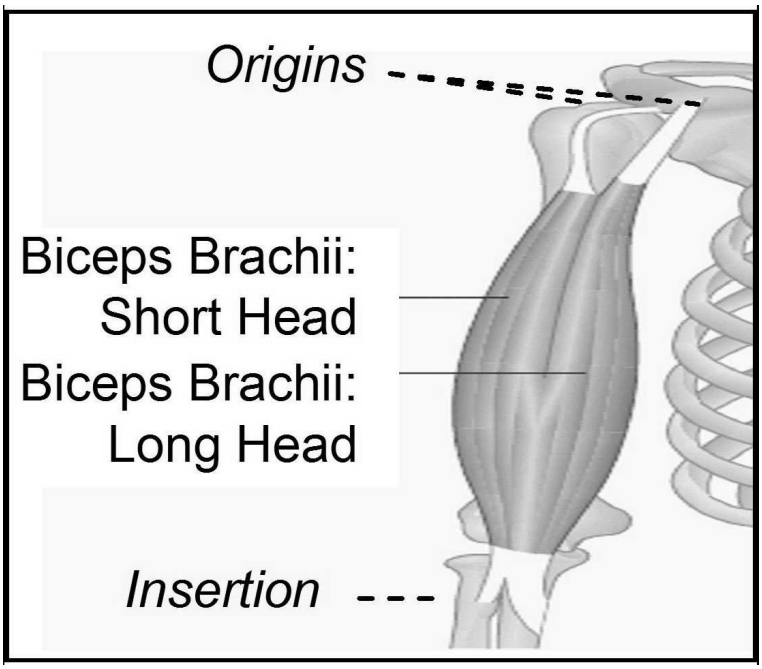

Figure 1: Anatomical drawing of the biceps brachii muscle (adapted from [29]).

muscle length does not change. This type of contraction can be experimentally tested in-vitro on a dissected muscle. But because of the semi-elastic properties of tendons, a constant muscle length can not be assured in-vivo. Therefore for this study an isometric muscle contraction is defined as a muscle contraction at which the joint angle of which the muscle is operating, does not change. The joint muscle of interest in this study is the biceps brachii, and the kinesiological articulation of interest is elbow flexion with an angle of 90 degrees (angle between the humerus and the ulna). In general, muscle fatigue has a complex nature during voluntary contractions. To produce voluntary contractions at least three major anatomical components are involved, the central nervous system, the peripheral nerve and neuromuscular junction, and the skeletal muscles. Fatiguing can be initiated at any one of these components. As it may be assumed, low force voluntary contractions can be maintained longer than high force contractions. Skeletal muscle is one of the most adaptable tissues in the human body. The main reason that skeletal muscle changes properties is to reflect

a change in the muscle activation level. For instance, muscles typically feel 'harder' during contraction due to a physiological change, the shortening of the acto-myosin filaments composing the striated muscle fibers [32]. With this being said, the macroscopic viscoelastic properties of muscles are directly related to the tension provided by the muscle fibers [45].

During muscle contraction there is a reduction in length along the long axis of the muscle contractile element [67]. Because the skeletal muscle can be modeled as having no change in volume during contraction [7], the shortening in the length along the parallel axis of the muscle is coupled with changes in the transverse axis dimension. The changes in the transverse axis dimension can be sensed at the skins surface.

1.1.2 Surface Mechanomyograms

During voluntary contractions, the dimensional changed in muscle fibers and muscle-tendon geometry [8, 46] produce natural muscle vibrations. Because of this low frequency (<100 Hz) and continuous surface mechanical oscillations, also called "muscle noise", are naturally generated by skeletal muscle. Typical sensors used to record these mechanical oscillations are skin-mounted accelerometers, condenser microphones, or laser displacement sensors [47, 61, 62, 69]. Independent of the type of sensors used, recordings of muscle mechanical oscillations with these sensors are called surface mechanomyograms (S-MMGs) (See. Fig 2)[46].

S-MMGs have been used recently for numerous muscle related objectives, for example; 1) muscle fiber typing in sports medicine [50] 2) to investigate the effect of neuromuscular diseases on the muscle [3] and 3) to investigate the effect of aging [23] on the muscle. S-MMGs appear to be a good index for force and fatigue for muscles [48, 16]. The amplitude of S-MMGs was shown to be highly correlated with the maximum of the second derivative of the force output, during the onset of muscle contraction. At the cellular level the second derivative of the force output is related

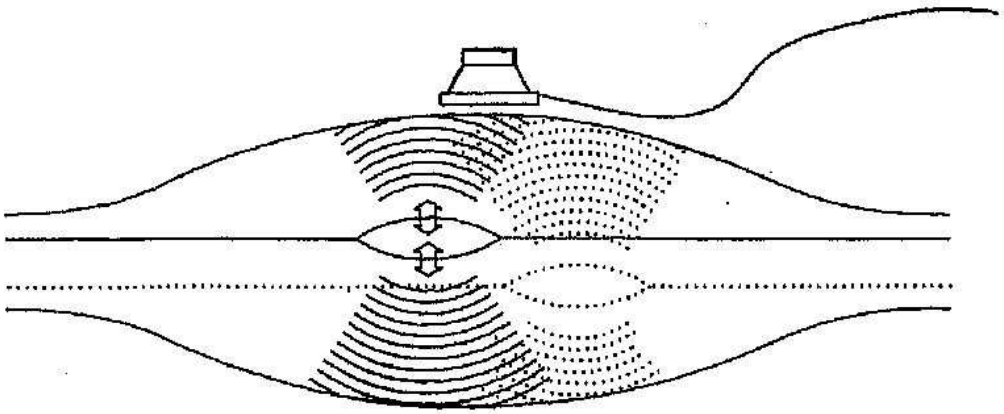

Figure 2: Schematic representation of the hypothesized MMG generation process resulting from vibrations generated by dimensional changes of the active muscle fibers during (fluctuations of) voluntary contractions ([46]).

to the amount of calcium ions released by the muscle cells [47]. Therefore, the second derivative of the force output is considered to be a good indicator of the muscle activation level. Hence, S-MMGs depend on specific aspects of the electromechanical coupling efficiency in muscles. The natural muscle vibrations recorded by S-MMGs can therefore be used to estimate non-invasively the muscle state and activity level in-vivo.

The physiological origin and time-frequency characteristics of S-MMGs depend on muscle structure, mechanical state, as well as the electromechanical coupling efficiency in muscles [6, 51, 63]. Indeed, the S-MMGs result from the non-linear summation of the active muscle fiber contractions [49, 68]. S-MMGs are also modulated by the architecture of the muscle-tendon complex, and the fat and skin layers. Typically, for isometric contractions at increasing effort level, the spectrum of the S-MMG signal exhibits an increase of its temporal root-mean square value along with a spectral shift towards higher frequencies [8]. These S-MMG variations are associated with a recruitment of faster motor units and an increase in firing rates of motor units [46]. Hence, S-MMGs have typically been used to monitor the muscles' mechanical activity (since the mechanical activity influences the S-MMG amplitude and frequency

content), thus providing complementary information to electromyograms (EMGs) which measure the muscle's electrical activity instead. But S-MMGs have rarely been used to estimate the mechanical properties (e.g. viscoelasticity) of skeletal muscles [42, 52]. However, since the S-MMGs correspond physically to propagating vibrations along the muscle, they appear as a potential tool for non-invasive study of skeletal muscle viscoelastic properties [56].

However, despite the large body of literature on S-MMGs, the spatial variations of S-MMG over a single muscle remain unclear since most studies have used only a single sensor, and the influence of the sensor location over the muscle of interest was investigated in only a few recent studies [52, 12, 14, 43]. Those studies, using a two dimensional array of accelerometers [42, 14, 24], have shown that the S-MMG amplitude and frequency content is indeed strongly influenced by the S-MMG sensor location over the studied muscles. Furthermore, the propagation directionality (e.g. transverse vs. longitudinal) and spatial origin (e.g. from motor points or from muscle extremities) of the S-MMG over the muscle is likely to vary depending on the type of tested muscle contractions (e.g. sustained voluntary contractions vs. direct electrical stimulation of motor twitch), but also on the frequency band which is analyzed. Hence, the physiological origin of S-MMG generation mechanism (e.g. force tremor vs. muscle fiber contractions) should be frequency-dependent [47]. Existing studies only partially address these issues, in particular regarding the frequency-dependency of the S-MMG spatial variations and S-MMG propagation directionality in the muscle [52, 14, 24, 13].

1.1.3 Current Elastography Techniques

Traditional palpation techniques, such as the modified Ashworth scale, can only provide a subjective assessment of muscle stiffness (or muscle tone) since the diagnosis often depends on the experience and subjectivity of each examiner [44]. On the

other hand, elastography techniques have been developed to provide objective measurements of the viscoelastic properties of skeletal muscles by mapping how these properties influence the physical characteristics (e.g., amplitude or velocity) of low-frequency mechanical vibrations [30] propagating along the tested muscles. Currently, standard elastography techniques are active since they rely on an external mechanical or radiation excitation source to generate these propagating low-frequency vibrations into skeletal muscles [30]. Typical sources are vibrating probes attached at one extremity of the muscle or the radiation force effect generated by focused ultrasonic beams inducing a mechanical push within the tissues. Consequently, implementing a near-real-time tomographic elastography system (i.e. similar to a CT scan) for imaging the spatial variation of the local viscoelastic properties along a whole muscle can potentially be challenging with active elastography techniques since multiple excitations would be needed at various locations over the muscle of interest. This could be achieved using several excitation sources simultaneously, or alternatively moving a single source along the muscle and assuming that the muscle condition is not changing between measurements. But, overall, such an experimental set-up would likely increase the complexity, duration and thus costs of future clinical protocols as well as potentially create discomfort for the patients.

1.2 Motivation and Goals

It has been demonstrated that coherent vibrations between sensor pairs, extracted from diffuse random wave fields or ambient noise measurements, can be used to estimate passively the local impulse response (or Green's function) of the propagating medium between these sensors by recent investigations in ultrasonics [66], seismology [59, 57] underwater acoustics [57] and structural health monitoring [56, 38]. Based on this approach, there is potential to develop a passive elastography technique which relies on extracting the fraction of coherent vibrations propagating between a pair

of skin-mounted sensors, from the cross-correlation time-function of their S-MMG records, in order to directly measure the local viscoelastic impulse response of the contracted skeletal muscle [56]. When yielding an estimate of the in-vivo viscoelastic impulse response along the muscle, the benefit of this approach when compared to conventional active elastography techniques is not needing an external mechanical or radiation source. Furthermore, when using an array of skin-mounted sensors (e.g. see Fig. 4), this passive elastography technique would allow for simultaneous elastography measurements between multiple sensor pairs since each S-MMG sensor potentially acts as a virtual in-vivo vibration source radiating along the muscle. Hence passive elastography could provide a simple, low cost means for tomographic elastography imaging of the spatial variations of the viscoelastic properties over a whole skeletal muscle.

One aim of this work was to investigate the directionality of the spatial coherence of propagating S-MMG in the biceps brachii muscle during submaximal isometric voluntary contractions by using a two-dimensional array of skin-mounted accelerometers (see Fig. 4). The S-MMG coherence, for a given sensor pair, is a frequency-domain measure of the similarity of the S-MMG signals propagating between those sensors. Studying the spatial variation of S-MMG coherence across all sensor pairs can be used to estimate how the S-MMG propagation directionality (i.e. longitudinal vs. transverse) vary across frequency, sensor separation distance and contraction level. Specifically, for high frequencies S-MMG ($f > 25\ Hz$) which are dominated by local muscle fiber activity [47], it is hypothesized that the S-MMG coherence is overall higher in longitudinal directionality (i.e. along the muscle axis) which corresponds to the main orientation of the biceps muscle's fibers. Even for lower frequency S-MMG ($f < 20Hz$), which are more dominated by whole limb vibrations, force tremor or bending transverse modal resonances, we expect to longitudinal propagation. In another aim of this work, the propagation directionality and spatial origin of the

coherent S-MMG was investigated to determine which sensor pairs could be used for implementing the passive elastography technique during voluntary contractions, since little information was available in the physiology literature [52, 13] on the spatial variations of S-MMG generated by skeletal muscle.

1.3 Thesis Organization

This thesis gives the detailed approach taken to accomplish the aims mentioned in section 1.2. Chapter 2 will discusses the experimental design used to complete the study. The chapter includes subject information, experiment setup and a detailed protocol used. Following that, Chapter 3 includes the detailed methods used to process the data. Then, Chapter 4 presents the results from the experiment, including raw data as well as processed data. This is accomplished by using figures and tables in order to present the data for interpretation. Chapter 5 discusses the results found in this study. It compares and contrasts the results to previous studies completed, as well as discuss the findings in comparison to the aims of this work. Chapter 6 draws conclusions based on the results from this work as well as the discussion. Chapter 7 brings forth recommendations for future work that will further advance the scientific knowledge of work in this field. The future works section will present ideas and next steps that will lead to a more complete understanding that is essential to fully understanding wave propagation in skeletal muscle.

1.4 Summary

Using skin mounted accelerometers is one way to measure the mechanical activity of skeletal muscle, called S-MMGs. This information could prove to be useful in giving supplemental information to EMG data, or in determining the in-vivo viscoelastic properties of skeletal muscle. This work is expected to provide an innovative technique in determining the directionality (transverse or longitudinal) of S-MMGs propagation

in skeletal muscle. This will be done by using two different but mathematically equivalent techniques to determine the spatial coherence of the S-MMG signals, frequency averaged coherence and cross correlation peak.

CHAPTER II

EXPERIMENTAL DESIGN

2.1 Subjects

Ten healthy male subjects (age: 29 ± 5 years, height: 175 ± 9 cm, body mass: 71 ± 8 kg), with no overt sign of neuromuscular diseases, volunteered to participate in the present study and signed an informed consent form. All subjects were right handed. The thickness of the skin and fat layer overlaying the biceps brachii muscle at each of longitudinal distance (0 - $4\Delta y$), ranged from 1.7 - 5.8mm when measured with ultrasound B-mode images (see Fig. 3 for examples). This study was conducted according to the protocol approved by the Institutional Review Board of the Georgia Institute of Technology.

2.1.1 Experimental Setup

All fifteen accelerometers were arranged on a 3 $\times$ 5 grid (see Fig. 4). The main biceps axis was determined based on anatomical landmarks for each subject as extending from the origin of the tendon of insertion (distally) to the coracoid process of the scapula (proximally) [29]. For each subject, the sensor grid axis (and thus imaging plane) was approximately aligned with the longitudinal axis of the biceps brachii, which corresponds to the muscle fiber orientation since the biceps has a simple fusiform architecture, at least in its lower section [53]. The transverse sensor spacing (i.e. along the medial-lateral direction) was set to $\Delta x = 2$ cm which was the smallest achievable separation distance given the sensor diameter ($\sim$1 cm). Since the tested biceps brachii muscles differed in length for each subject, the longitudinal spacing distance Δy (i.e. along the proximal-distal direction) between adjacent accelerometers was determined as 8% of the estimated length (L_m, with $26cm < L_m < 34cm$)

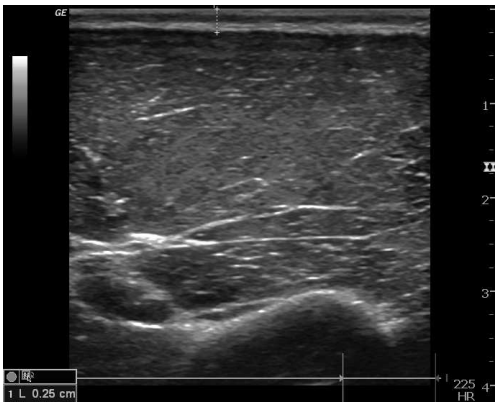

(a)

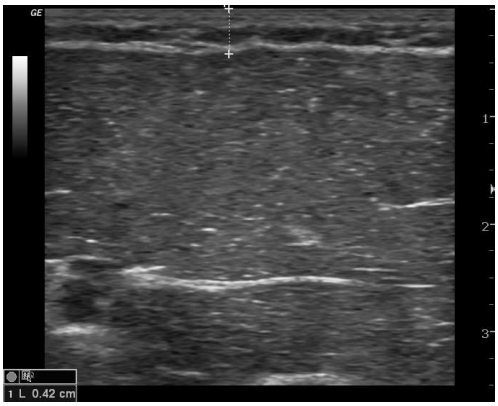

(b)

Figure 3: Example of skin and fat layer measurement with B-mode ultrasound images a) 0.25 cm b) 0.42 cm

of the biceps brachii long head muscle, following a previous approach [53, 55]. In this study, Δy varied from 2.1 cm to 2.7 cm for the tested muscles, to ensure that the accelerometers were placed in anatomically comparable positions on each subject's biceps brachii muscle. Consequently in all cases, the 3x5 sensor grid covered the region between 18% and 50% of L_m, where the coordinate origin was set at the distal end (0% of L_m) [53].

Fifteen miniature single-axis accelerometers (PCB® A352C65, mass=2 g, base diameter=9.5 mm, sensitivity=100 mV/g) were used with thin flexible cables to reduce drag (<1 mm diameter) to record S-MMG over the biceps muscle (as seen on Fig. 4). The accelerometers were skin-mounted over the biceps brachii using double-sided

medical tape to provide good contact while minimizing mounting artifacts and allowing for the muscle to move freely without any addition pressure interference, thus yielding reliable S-MMG signals as shown in previous studies [56]. Skin-mounted accelerometers allow for very sensitive measurements of local muscle vibrations (accelerations here) with the advantage of automatically tracking any muscle motion since they are attached to it, but with the potential disadvantage of causing mass loading artifacts.

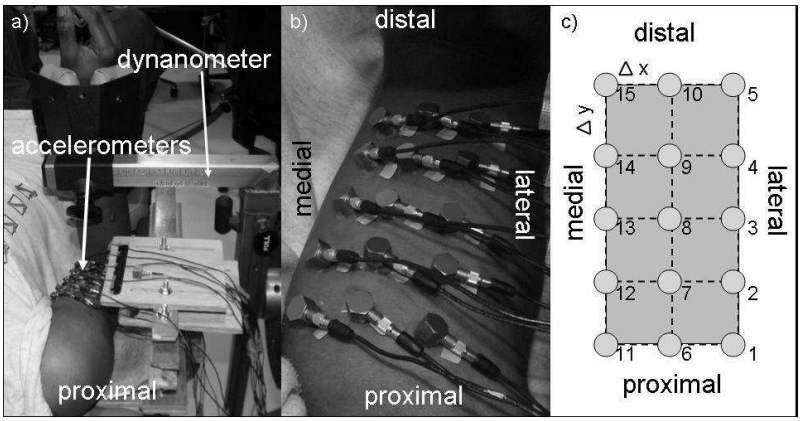

Figure 4: a) Experimental set-up for isometric elbow flexion tests (without sensor). b) Top view with skin-mounted accelerometers. c) Schematic of the 15 accelerometers locations.

2.2 Experimental protocol

All 15 channels were perfectly time synchronized with a sampling frequency of 1 kHz on a Compact DAQ system (National Instrument®, Austin, TX see Fig. 5).

For each subject, S-MMGs were recorded over the biceps brachii muscle during short ($t = 10\ s$) voluntary isometric contractions (elbow flexion) which allows for a constant muscle torque output and relatively static experimental conditions. The computer-controlled dynamometer HUMAC (CSMi Medical Solutions, Stoughton, MA) was used as a platform. Each subject was situated laying on their back with

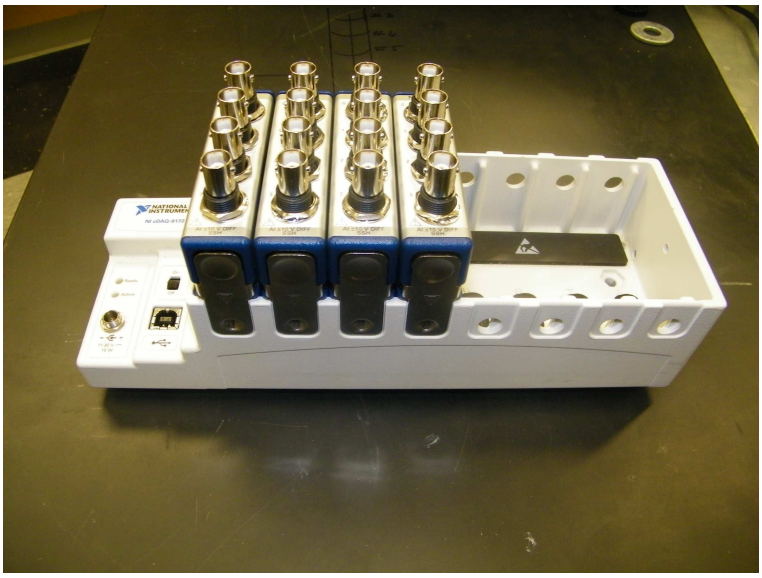

Figure 5: National Instrument Data Acquisition System.

their right arm attached to the dynamometer at the wrist (see Fig. 1(a)). The elbow joint was flexed at 90 degrees and the wrist was oriented in the neutral position. The right arm was immobilized horizontally using a supporting stand to minimize motion artifacts. The rotation axis of the elbow joint was visually aligned with the rotation axis of the HUMAC dynamometer. The force output of the biceps was recorded independently by a force transducer attached to a bar at the subject's wrist. As seen in Fig. 1(a), the accelerometer cables were attached to a board that was extended from a vertical platform. The board was extended so that it minimizes the length of the cables extending from the accelerometer before the cables where attached to a stable structure, which minimized the drag of the cable on the accelerometers. A preliminary study has confirmed that this configuration isolated the accelerometers from the vibration caused by the subject's contraction by comparing the amplitude of vibration of the board to the amplitude of vibration being measured on the muscle and on the dynamometer. See Figure 6 for equipment flow of experimental setup.

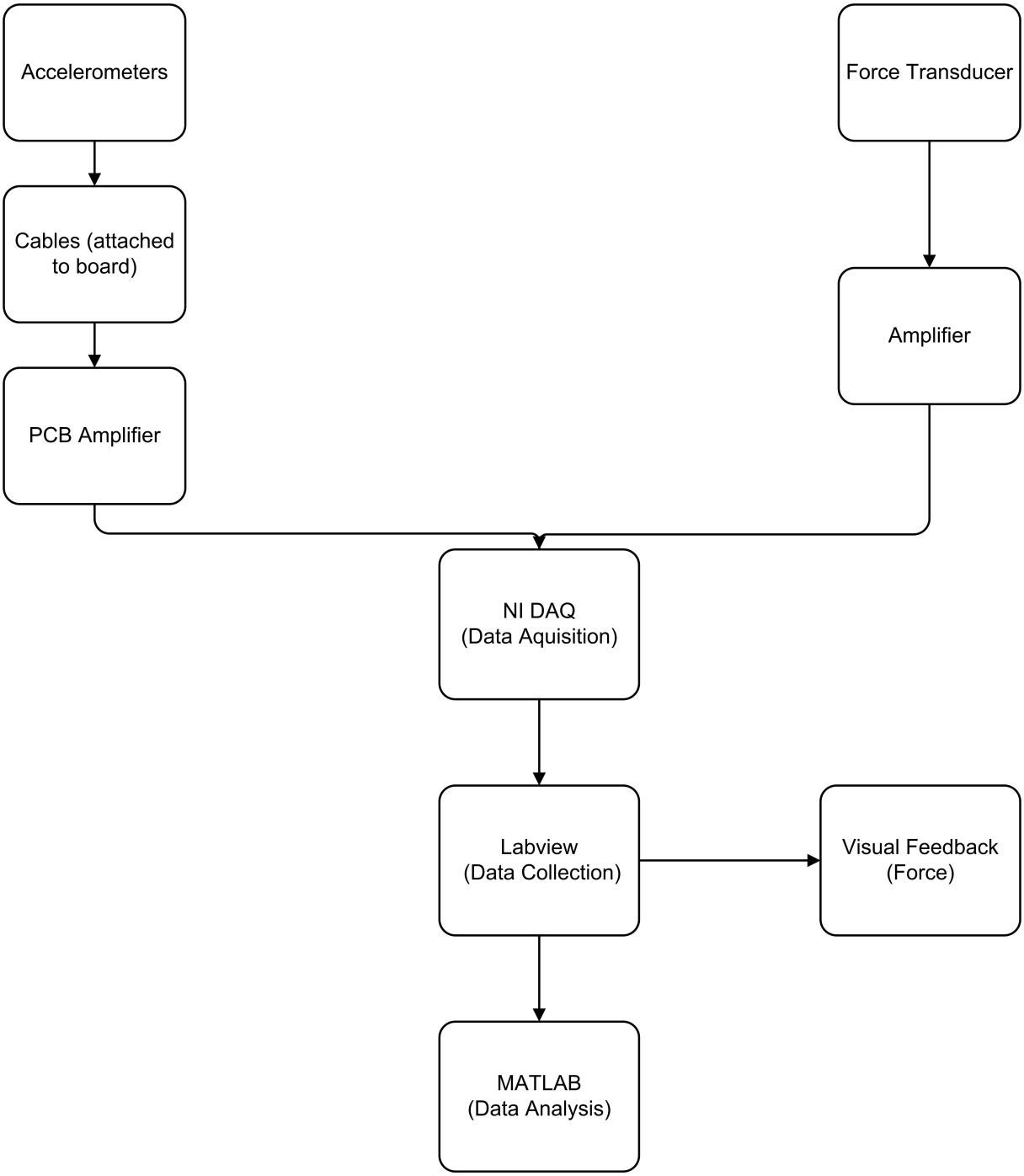

Figure 6: a) Flow chart depicting equipment flow of the experimental setup used for this study.

For each subject, the maximum voluntary contraction (MVC) force was determined based on the maximum force output measured over 3 brief maximal contractions. Thereafter, subjects performed submaximal isometric contractions, in which

they were asked to produce and maintain 20%, 40%, 60% (see Fig. 7) of maximal voluntary contraction (MVC) force for 10 s while facing a video monitor displaying torque output as visual feedback. Subjects were encouraged to rest and relax for 3 min between each contraction to minimize artifacts due to muscular fatigue. A total of three trials were performed by selecting a randomized order of contraction levels.

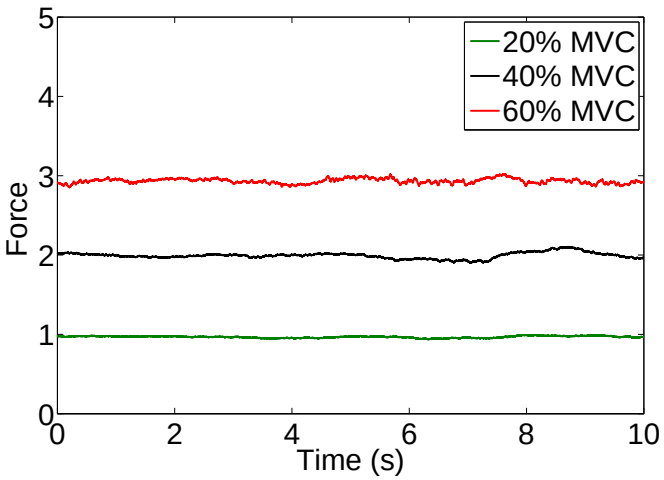

Figure 7: Example of force recording from Subject 9 Trial 1.

2.3 Limitations

There were a few limitations encountered during the experimental setup and experimental protocol design. One limitation found was that the accelerometers have two drawbacks when being used in under these conditions; 1) the cables that are attached to the accelerometers may have caused some drag on the accelerometers and 2) the weight of the accelerometers may be interfering with the measurements of the S-MMGs. Using a laser vibrometer could potentially solve these limitations, but it would also introduce new limitations that the accelerometers can overcome. The accelerometers have the advantage of being attached to the skin, therefore they have a better change of measuring signal from the same point on the muscle even

if the muscle moves. With non-contact methods, such as the laser vibrometer, the measurements would be from a completely different point if the subject moves.

2.4 Summary

Fifteen miniature accelerometers were used to measure S-MMGs on 10 healthy male subjects, with approval from the Georgia Institute of Technology Institutional Review Board. A two dimensional 3×5 grid of accelerometers were placed on the subjects arm between 18% and 50% of the subjects L_m. Subjects were asked for 3 trials to contract at 20%, 40% and 60% of the MVC for 10 s. Limitations that include mass loading artifacts and drag from the cables were found when designing this experiment.

CHAPTER III

METHODS

3.1 Data Pre-processing

Data was filtered in the frequency band (5 Hz - 100 Hz) and amplified with a gain of 200×. Figure 8(a) shows the raw S-MMG collection before any data processing. The contraction level of 40% MVC (red) is plotted with the baseline of 0% MVC (black) to show the difference in acceleration amplitude during an isometric voluntary contraction. Notice the low frequency oscillations in both recorded S-MMG signals. During the signal processing a 2nd order Butterworth filter was used to filter out data outside of a 5 Hz to 100 Hz freqency range. The zero mean of the signal in Fig. 8(b) shows that this process filtered out the low frequency signal that arose from whole limb motion. The fact that the two signals are 'zero mean signals' is critical in determining the coherence between two signals.

The mean power frequency (f_{MP}) of the recorded signal is defined by Kwatny et al. [37] as

$$f_{MP} = \frac{\int_{f_1}^{f_2} f G_{xx}(f)}{\int_{f_1}^{f_2} G_{xx}(f)} \tag{1}$$

where $G_{xx}(f)$ is the power spectrum of the signal $x(t)$, f is the frequency, f_1 =5 Hz and f_2 =250 Hz. The f_{MP} of each of the 15 sensors was calculated according to Eq. 1 for each trial and contraction level.

These values were then averaged over the 15 sensors and 3 trials which gave a value corresponding to one subject for each contraction level. Fig. 9 shows this value averaged across all 10 subjects with the error bars indicating one standard deviation. The results show that as contraction intensity increases, f_{MP} also increases, which is

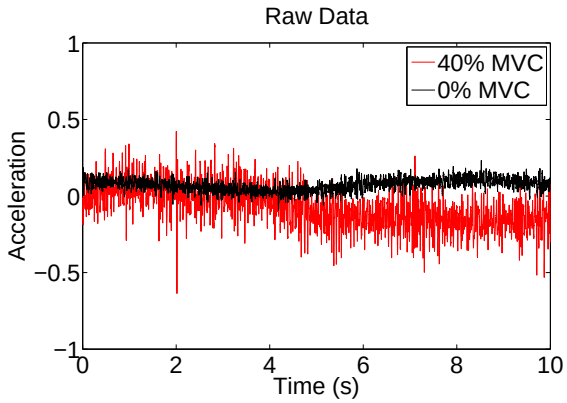

(a)

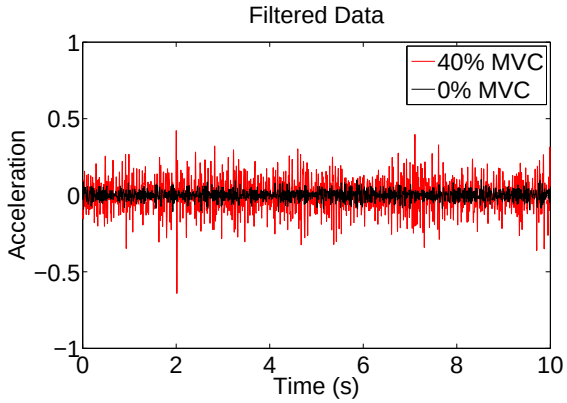

(b)

Figure 8: S-MMG data vs. time for sensor #8 at 0% MVC (baseline) and 40% VMC) for a) raw (non filtered) and b) filtered between 5 Hz and 100 Hz for Subject 10 trial #1 .

consistent with a previous study done using accelerometers to measure S-MMGs over the biceps brachii muscle during isometric contractions [33].

As an illustration, Fig. 10(a) shows the power spectrum (of sensor #8 for subject 1 and trial 1) across frequency for increasing contraction level. Compared with the noise in the resting muscle (0 %MVC), the power increased as contraction level increased.

The signal to noise ratio was defined as the power ratio between the meaningful S-MMG (measured signal at a contraction level greater than 0% MVC) and noise (measured signal at rest). The power was averaged between 5 Hz - 250 Hz for each signal. The S-MMG measured at each sensor was averaged over the 15 sensors for

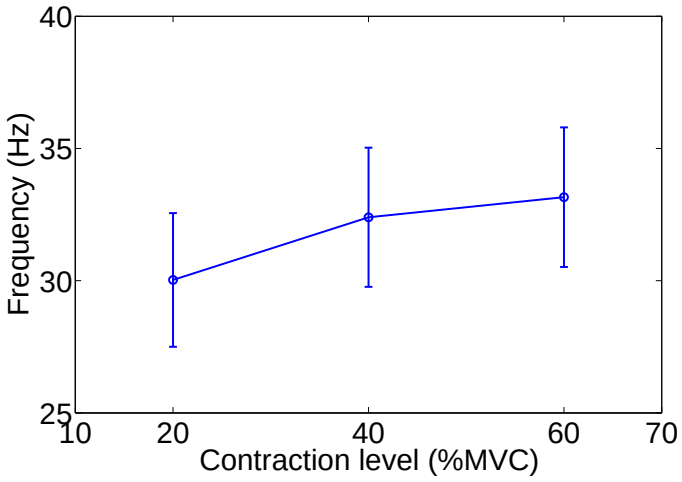

Figure 9: Average mean power frequency (f_{MP}) of S-MMG across 10 subjects for 3 different contraction levels (20%, 40% and 60% MVC).

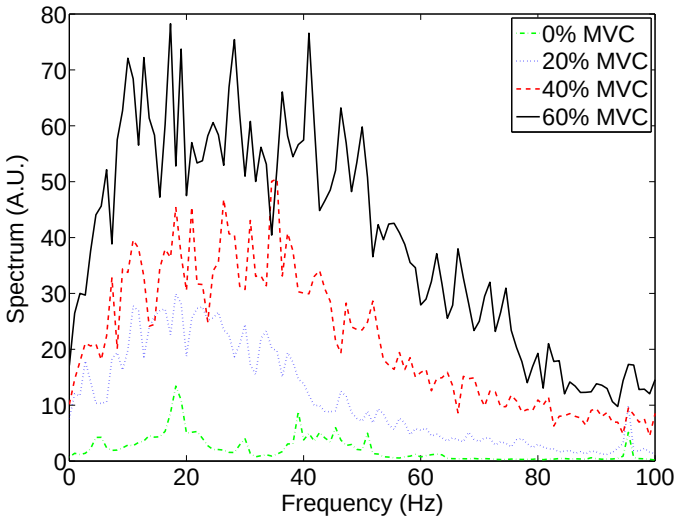

(a)

Figure 10: Power spectrum for subject 1 measured on sensor # 8 for varying %MVC.

a single trial. This value was then averaged over the three trials, in order to obtain a value for each subject at each contraction level. These values were then averaged across the 10 subjects to obtain the mean and standard deviation for each contraction level. The signals obtained from the S-MMGs were found to be with high signal to noise ratio (see Fig. 11(a)). Compared with the noise in the resting muscle (0 %MVC),

the signal to noise ratio increased as contraction level increased ($P < 0.01$).

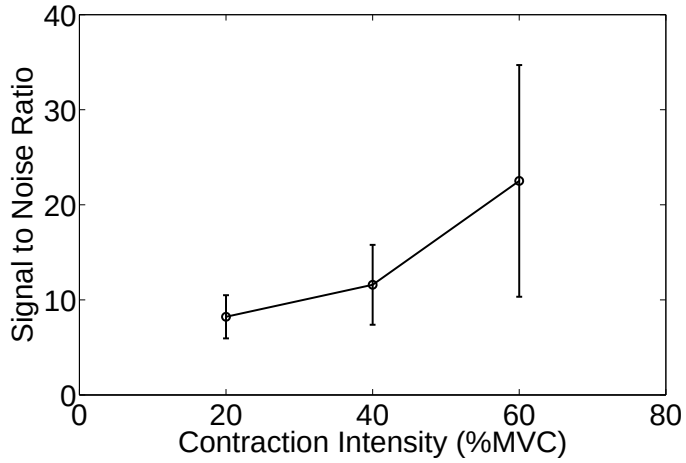

(a)

Figure 11: Signal to noise ratio across all recorded signal varied by contraction level (error bar is one standard deviation)

3.2 Signal Processing Techniques

The spatial coherence of two S-MMG signals can be determined from two different methods, this section will explore the background on the different methods. First, the similarity in the frequency domain between two S-MMG signals $x(t)$ and $y(t)$ recorded at different locations along the longitudinal axis of the muscle, can be estimated from the square of the magnitude of their coherence $\mid C_{xy}(f) \mid^2$, defined as [15]

$$\mid C_{xy}(f) \mid^2 = \frac{\mid G_{xy}(f) \mid^2}{G_{xx}(f)G_{yy}(f)} \tag{2}$$

where f is the frequency of interest, $G_{xx}(f)$ (resp. $G_{yy}(f)$) is the power spectrum of the signal $x(t)$ (resp. $y(t)$), and $G_{xy}(f)$ is the cross power spectrum of those two signals. The cross-power spectrum is defined as the Fourier transform of the cross correlation function of the two signals $x(t)$ and $y(t)$ [15]. The squared magnitude coherence between the two sensors was estimated using the "mscohere" Matlab® function [1], and results in a value between 0 and 1, with 1 meaning perfectly similar

and 0 meaning no similarity. In the remainder of this paper the quantity $\mid C_{xy}(f) \mid^2$ will be referred to as the magnitude squared coherence.

For each test, the first and last .25 s were clipped from the signal, meaning the total signal time of 9.5 s was used to calculate the coherence between pairs of S-MMG signals(see Eq. (2)). The power spectrum and cross-spectrum of the recorded S-MMG were estimated by segmenting the S-MMG time series in overlapping windows ($N = 1100$ points long with 50% overlap) and the number of samples for the fast fourier transform operation was selected as 256. Confidence intervals of the coherence function can be estimated to achieve a desired level of significance, based on an analytical expression of the variance of the coherence [11, 10]. The confidence level cl of the coherence function, at the α quantile is given by [31]

$$cl = 1 - (1 - \alpha)^{\frac{1}{L-1}} \tag{3}$$

where L is the signal duration multiplied by the sampling frequency of the recording ($Fe = 1000\ Hz$) divided by the window length ($N = 1100$ points). Such that

$$L = \frac{(T)(Fe)}{N} = \frac{(9.5\ s)(1000\ Hz)}{1100} = 8.6364 \tag{4}$$

In this study the confidence level was set to $cl \approx 0.32$ using Eq. (3), based on the selected parameters $\alpha = 0.95$, $L = 8.6364$.

At each contraction level (%MVC) the frequency-averaged coherence $\mid C_{xy}(f_c) \mid^2$, for varying center frequency f_c was defined as:

$$\mid C_{xy}(f_c) \mid^2 \simeq \int_{f_c-\Delta f}^{f_c+\Delta f} \mid C_{xy}(f) \mid^2 \mathrm{d}f \tag{5}$$

where Δf=2 Hz.

Another method to calculate the similarity between two S-MMG signals $x(t)$ and $y(t)$ recorded at different locations is by using the time-domain cross-correlation function. The cross-correlation function is approximately equal to the frequency averaged

coherence of two signals, as the frequency band of interest approaches 0 [26]. With continuous time signals the normalized cross correlation function between two S-MMG signals $x(t)$ and $y(t)$ is defined by

$$R_{xy}(\tau) = \frac{\int_{-T/2}^{T/2} x(t)y(t+\tau)\mathrm{d}t}{\sqrt{\int_{-T/2}^{T/2} x^2(t)\mathrm{d}t \int_{-T/2}^{T/2} y^2(t)\mathrm{d}t}} \tag{6}$$

where the signals $x(t)$ and $y(t)$ both filtered with a bandpass filter with a frequency band of $f_c \pm \Delta f$ with Δf=2 Hz. The function is normalized between +1 and 0, where +1 indicates a perfect similarity between the two signals and 0 indicates no similarity. The cross correlation peak X_{xy} is then defined as

$$X_{xy}(f_c) = max(R_{xy}(\tau)) \tag{7}$$

The two signal processing techniques described above can be used to determine the spatial coherence. Fig. 12 gives a flow chart that details the steps taken on the two different routes to determine the spatial coherence.

3.3 Spatial Coherence Technique to Determine Directionality

Recall from Section 3.2 that there are two separate processes used to determine the spatial coherence of two S-MMG signals. Using the fact that the spatial coherence values vary between 0 and 1, (with 0 meaning no similarity and 1 being completely similar) the directionality of S-MMG propagation can be determined by comparing spatial coherence on longitudinal pairs versus transverse pairs. Before this was accomplished the understanding of the main effect of several factors that influence the S-MMG spatial coherence was investigated. A 15 × 15 color coded matrix of spatial coherence values will be used to analyze the directionality. In this matrix, the 5 × 5 square boxes located on the diagonal from the lower left to the upper right denotes

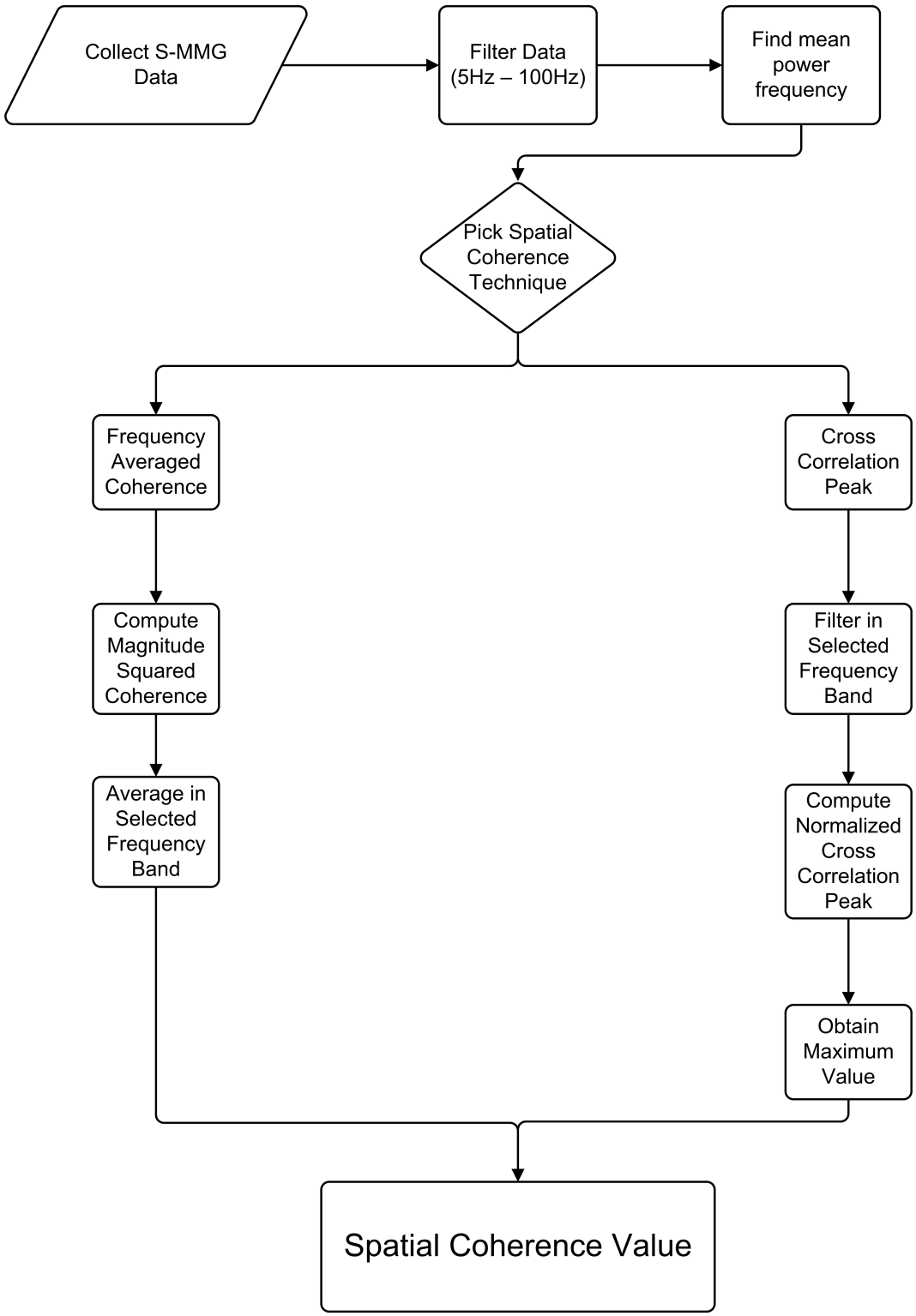

Figure 12: a) Flow chart depicting the two processes use in order to determine the spatial coherence.

sensor pairs on the same longitudinal line. The main effect of the factor alone averaged across the levels of the other factors, was investigated. The factors investigated were frequency, sensor separation distance (2,4,6 and 8 cm longitudinal direction and 2 and 4 cm transverse direction), contraction level (20, 40 and 60% MVC) and sensor orientation (longitudinal vs transverse). With the frequency as the main effect all other factors were averaged, but the sensor orientation was kept separate. For the remaining factors the frequency was averaged in a 4 Hz frequency band centered about f_{MP} while the other factors were averaged across all levels.

3.4 Statistical Analysis

Statistical analysis was performed to determine if there was statistical significance to the values of f_{MP}, which showed to increase as contraction level increased. The f_{MP} was found for each sensor and averaged across all 15 sensors for each trial. The 3 trials were then averaged to give a single f_{MP} for each subject at each contraction level. These values were then averaged and plotted with the error bars indicating one standard deviation. A one way analysis of variance (ANOVA) was used to determine statistical significance with the dependent variable being spatial coherence and the independent variable being contraction level. Three separate one-way ANOVA test were performed in order to asses the influence on spatial coherence of 3 different factors; frequency, sensor separation distance and contraction level. For the frequency analysis longitudinal and transverse sensor pairs were kept separate, while they were averaged across trials, subjects, sensor separation distance and contraction intensities. The coherence value at 10 Hz intervals was used to determine statistical significance. Determining the main effect of the sensor separation distance was done by averaging the spatial coherence across trials, subjects and contraction level. To determine the effect of contraction level on the spatial coherence, the spatial coherence values were averaged across, trials, subjects and sensor separation distances. An alpha level of

0.05 was used for all statistical comparisons, where appropriate $P < 0.05$ and $P < 0.01$ was noted. Unless otherwise stated the error bars in the figures represent one standard deviation.

3.5 Summary

There was a gain of 200× applied to the signal and the data was found to have a good signal to noise ratio for all force levels tested, and it was then filtered between 5 Hz and 100 Hz. The method to determine propagation directionality of the S-MMG waves generated by involuntary contraction was to investigate the main affect of sensor orientation direction. This was done by averaging the frequency across a 4 Hz frequency band and averaging the remaining factors across all levels. For statistical significance, and alpha value of 0.05 was used in a one-way ANOVA for the main effects.

CHAPTER IV

RESULTS

The Fast Fourier Transform (FFT) of the S-MMG data gives us the frequency content of the recorded signal. This information revealed the importance of the frequency content of the data, which showed that there was no significant signal past 65 Hz when compared to the baseline. Figure 13 shows the frequency content of sensor #8 at 40% MVC and at 0% MVC (baseline). It can be seen that there is a high amount of activity below 10 Hz which may be attributed to muscle tremor. After about 12 Hz there is activity that can be attributed to the muscle "noise" generated during a voluntary isometric contraction.

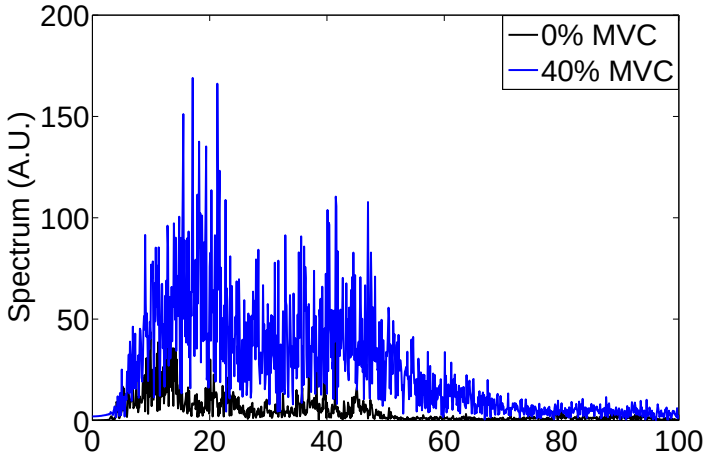

Figure 13: FFT of the filtered time domain S-MMG data for subject 10, trial 1, sensor #8 (at 0% MVC (baseline) and 40% MVC)

4.1 Directionality Analysis

Fig. 14 illustrates the influence of various parameters such as contraction level, sensor separation distance and sensor pair orientation (e.g. longitudinal vs. transverse)

on the frequency-dependency of the computed S-MMG coherence for all subjects. Figures 14(a) and 14(c) contrast the effects of sensor pair orientation and distance on the S-MMG coherence function. Figure 14(a) shows the coherence function between the reference sensor #6 and the four other sensors $\#7 - \#10$ aligned along the same vertical grid line (i.e. longitudinal direction) and Fig. 14(c) displays the coherence function between the reference sensor #3 and the two other sensors $\#8 - \#13$ aligned along the same horizontal grid line (i.e. transverse direction) (see Fig. 4(c)) at 40% MVC. Fig. 14(a) shows that the coherence values decrease for increasing frequencies and increasing sensor separation distance, as expected from theoretical predictions. The coherence values remain significant (i.e. > 0.32, see Eq. (3)) over a wider frequency range for sensor pairs oriented in the longitudinal direction, i.e. along the muscle fiber direction (Fig. 15(a), 62.38 $\pm$ 4.54 Hz), when compared to sensor pairs oriented in the transverse direction (Fig. 15(b) 31.70 $\pm$ 3.88 Hz), i.e. across the muscle fiber direction. Fig. 14(b) and Fig. 14(d) illustrate how S-MMG spatial coherence vary for increasing contraction level for two sensor pairs aligned either along the longitudinal (pair $\#7 - \#9$, 4.2cm$< 2\Delta y <$5.4cm) or transverse (pair $\#3 - \#13$, $2\Delta x =$4cm) direction but having a similar separation distance. The frequency value at which the coherence drops belows the significant value (0.32 denoted by dashed horizontal line) increased as contraction level increased in the longitudinal direction (Fig. 14(b)) although not in the transverse direction (Fig. 14(d)). Overall, Fig. 14 shows that the spatial coherence of S-MMGs can vary significantly with the contraction level and sensor pairs orientation, especially at higher frequencies ($f > 20$ Hz). Hence, the dependency of the spatial coherence S-MMG on each of the various aforementioned parameters are investigated systematically in the subsequent figures.

Figure 15 shows the coherence with frequency as the main effect for the longitudinal direction (Fig. 15(a)) and the transverse direction (Fig 15(b)). For sensor pairs

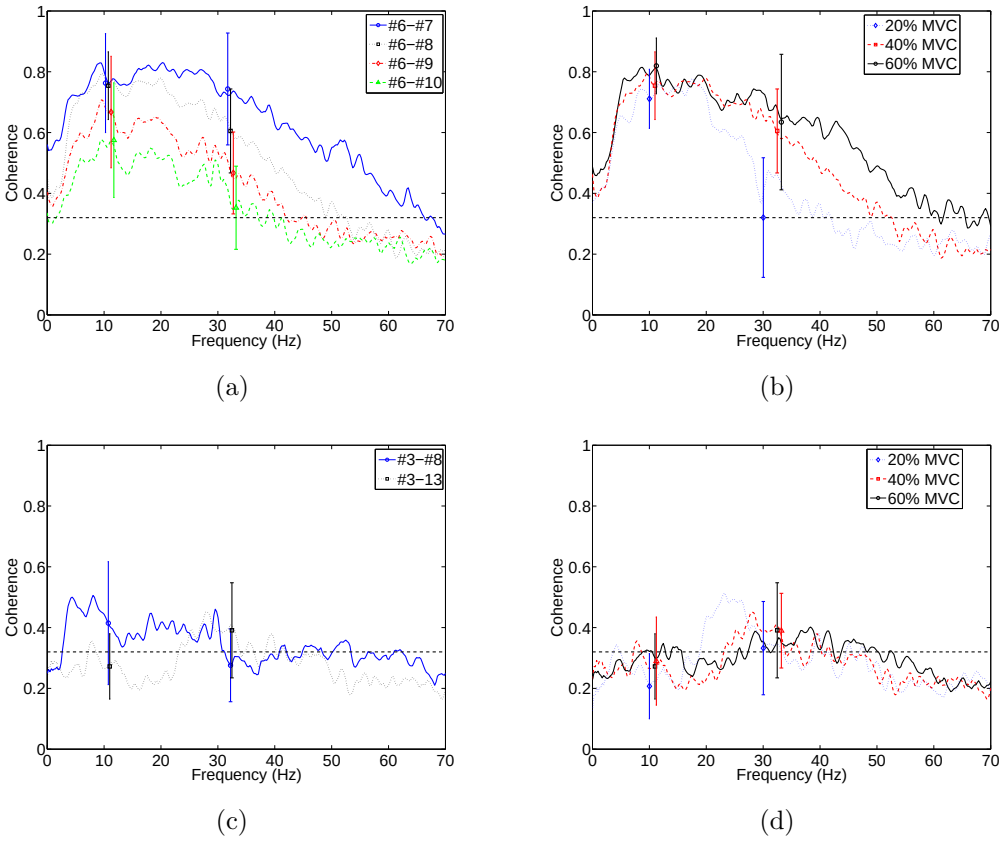

Figure 14: S-MMG coherence averaged over the 10 subjects at the same contraction level (40 % MVC) for increasing separation distance between pairs of skin mounted accelerometers located on the (a) central longitudinal sensor line (b) central transverse sensor line (see Fig. 1(c)). S-MMG coherence at a fixed distance r, for increasing % MVC between a pair of skin mounted accelerometers located on the center (c) longitudinal sensor line (sensor pair $\#7 - \#9$) (d) transverse sensor line (sensor pair $\#3 - \#13$, $r = 4$ cm).

oriented in the longitudinal direction coherence was found to decrease with increasing frequency ($P < 0.01$). The coherence in the transverse direction was also found to decrease as frequency increased ($P < 0.05$). The frequency at which the coherence drops below the significant coherence threshold of 0.32 (cut-off frequency, denoted by horizontal dashed line) for all longitudinal pairs was 62.38 ± 4.54 Hz, which was significantly different from all transverse pairs at 31.70 ± 3.88 Hz ($P < 0.01$). The cut-off frequency was averaged across all contraction levels, sensor separation distances and subjects.

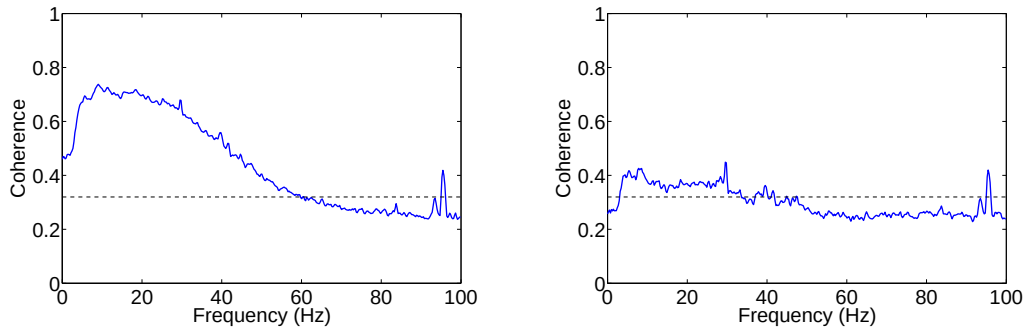

(a) (b)

Figure 15: S-MMG coherence averaged across all 3 contraction intensities, all 10 subjects and (a) all sensor pairs oriented in the longitudinal direction (b) all sensor pairs oriented in the transverse direction.

Figure 16 displays a matrix in a checkerboard format, showing the typical variations of the frequency averaged coherence function (Figs. 16(a) and 16(b)) and the peak value of the normalized cross correlation (Figs. 16(c) and 16(d)) of S-MMGs between all sensor pairs (see Eq.(2) and Eq.(6)). For each sensor pair the frequency averaged coherence values were averaged in 4 Hz frequency bands (see Eq.(5)) and the cross correlation was filtered in a 4 Hz frequency band, centered respectively at one third of the mean power frequency (low) and at the mean power frequency (high) . For each checkerboard matrix, the spatial coherence values were averaged across all 10 subjects and across 3 trials. It can be seen that at both low frequency ($\frac{1}{3}f_{MP}$, Figs. 16(a) and 16(c)) and high frequency (f_{MP}, Figs. 16(b) and 16(d)) the checkerboard has higher values concentrated along a 5×5 diagonal. These correspond to 5 sensors located on the same vertical grid line (medial, central or lateral, see Fig. 1(c)).

An analysis was performed that compared the frequency averaged coherence $\mid C_{xy}(f_c) \mid^2$ and the cross correlation peak $X_{xy}(f_c)$ between pairs of sensors with the same inter sensor separation distance along an individual longitudinal line (medial, central or lateral). The spatial coherence values computed for all 3 longitudinal lines were very comparable within 4% of each other. Hence, it was concluded that the

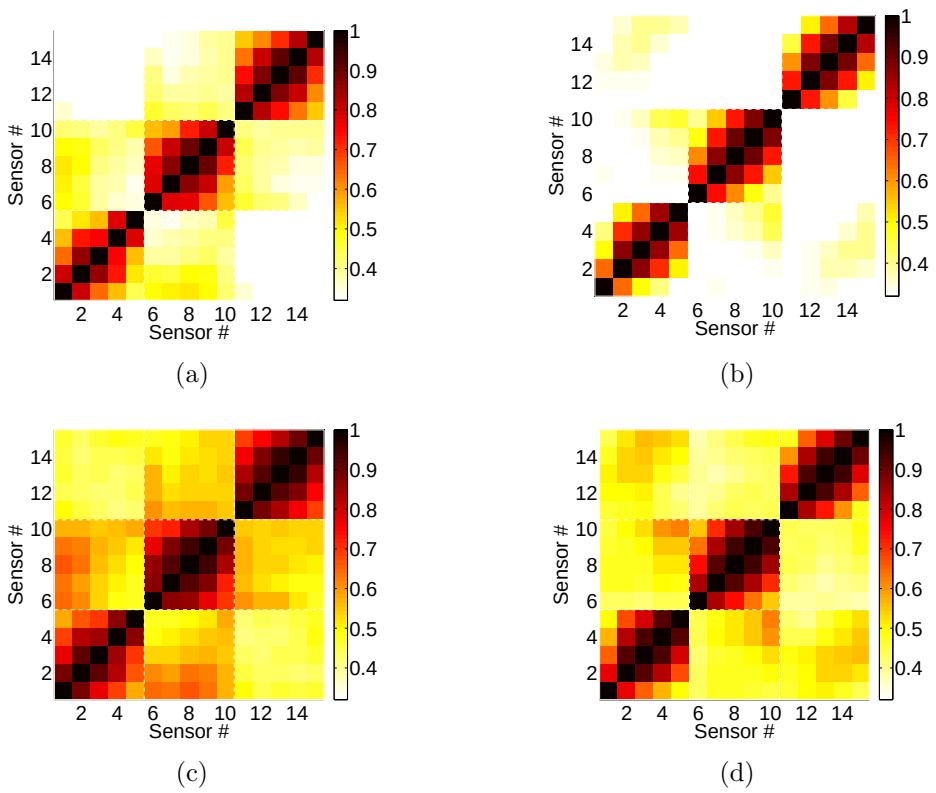

Figure 16: Mean value of the spatial coherence at 40% MVC between all sensor pairs averaged in a 4 Hz frequency band (see Eq. (5)) centered at (a) $\frac{1}{3}f_{MP}$ and (b) f_{MP}. Maximum value of the normalized cross correlation at 40% MVC between all sensor pairs average in a 4 Hz frequency band centered at (c) $\frac{1}{3}f_{MP}$ and (d) f_{MP}.

values for the three lines were not statistically different, therefore for Fig. 17 the values along the three lines were averaged together. At a given center frequency $f_c = \frac{1}{3}f_{MP}$ (Figs. 17(a) and 17(c)) or $f_c = f_{MP}$ Figs. 17(b) and 17(d)) and contraction level, Fig. 18 displays the mean and standard deviation values obtained after averaging all computed longitudinal coherence values (along medial, central and lateral lines) using Eq. (5) and Eq. (6) for all analyzed 9.5 s long S-MMG epochs (see section 2.2) and all subjects. Figure 18 display the mean variation of the frequency-averaged coherence values (at 40% MVC) for increasing sensor separation distance, for the same low and high frequency bands centered respectively at $\frac{1}{3}f_{MP}$ and at the f_{MP} as in Fig. 16. These computed values were averaged both over all 10 subjects with 3 trials and over

all equidistant longitudinal sensor pairs for increasing normalized separation distance from Δy to $4\Delta y$ ($2.1\ cm \leq \Delta y \leq 2.7\ cm$ (see Section 2.2)). Figure 18 confirms that the frequency-averaged coherence value and the cross correlation peak (in a 4 Hz frequency band) centered both at $\frac{1}{3}f_{MP}$ and at the f_{MP}, decreased as the sensor separation distance increases, as previously observed (see Fig. 14).

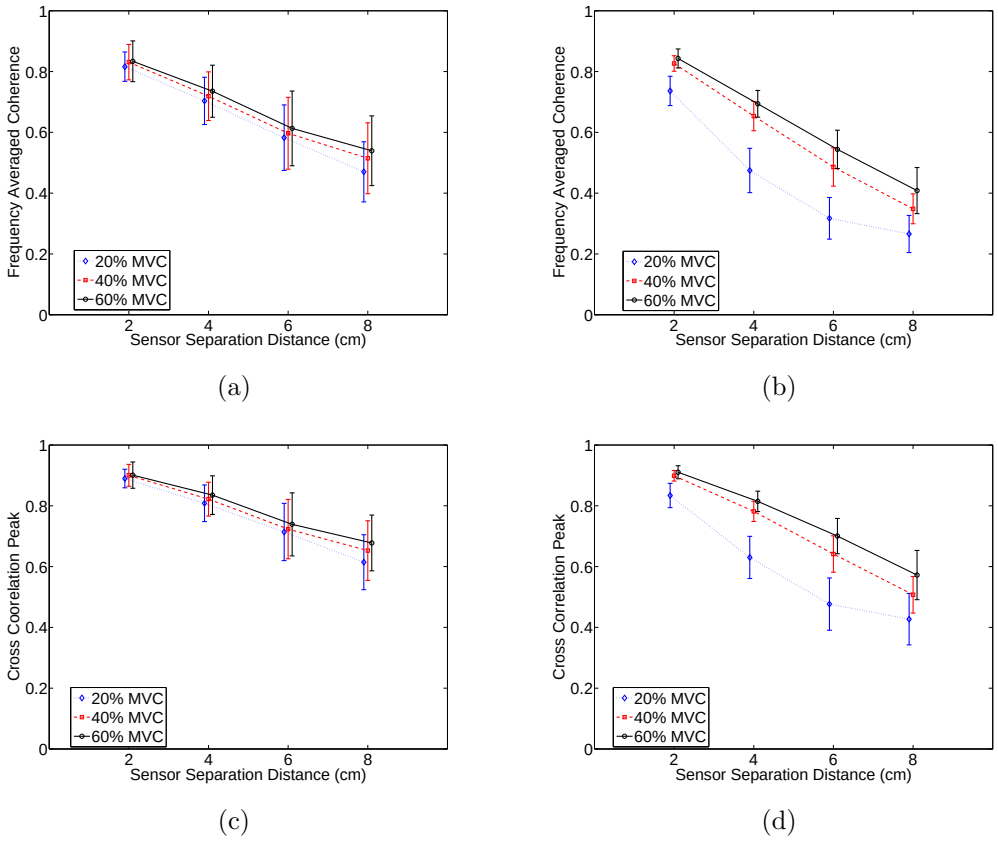

Figure 17: Coherence value averaged in 4 Hz frequency band at different contraction levels (% MVC) for increasing sensor separation distance at (a) $\frac{1}{3}f_{MP}$ and (b) f_{MP}. Cross correlation peak value filtered in 4 Hz frequency band at different contraction levels (% MVC) for increasing sensor separation distance at (c) $\frac{1}{3}f_{MP}$ and (d) f_{MP}. Error bars indicate one standard deviation over all 10 subjects and sensor separation distance combinations.

An analysis was performed to show the main affect of sensor separation distance on spatial coherence, measuring the spatial coherence for all equidistant sensor pairs from Δy to $4\Delta y$ ($2.1\ cm \leq \Delta y \leq 2.7\ cm$) and from Δx to $2\Delta x$ ($\Delta x = 2.0\ cm$)

(see Section 2.2)). The spatial coherence values were averaged across trials, subjects and contraction level. The sensor separation distances were averaged for all sensors with a common separation distance, along the same line. Figure 18(a) shows that the coherence decreases with increasing distance ($P < 0.01$) for sensors located on the same longitudinal line (medial, central and lateral). Figure 18(b) shows the coherence for increasing sensor separation distance for sensors pairs oriented on the same transverse line. There was no statistically significant difference in the spatial coherence at 2 cm when compared to 4 cm. In each figure, the error bars indicate one standard deviation from the mean.

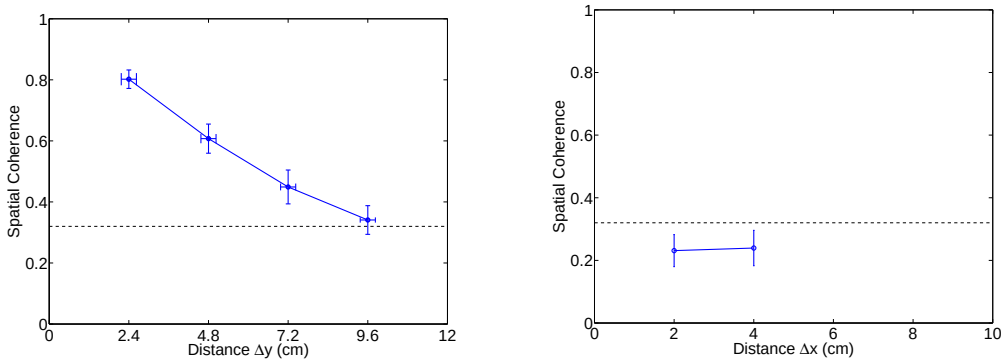

(a) (b)

Figure 18: Coherence value averaged in 4 Hz frequency band at f_{MP} for increasing sensor separation distance (a) in longitudinal direction and (b) transverse direction. Error bars indicate one standard deviation over all 10 subjects.

The spatial coherence is also dependent on contraction level. Figure 19 will explore the main affect of contraction level on the spatial coherence values for both longitudinal (Fig. 19(a)) and transverse (Fig. 19(b)) sensor orientation direction. The coherence values were averaged across trials, subjects and sensor separation distances for sensors pairs along the same line. For the longitudinal direction, Fig. 19(a) shows that the spatial coherence increases as contraction level increases ($P < 0.01$). There was no statistically significant difference in spatial coherence across contraction level for sensor pairs in the transverse direction.

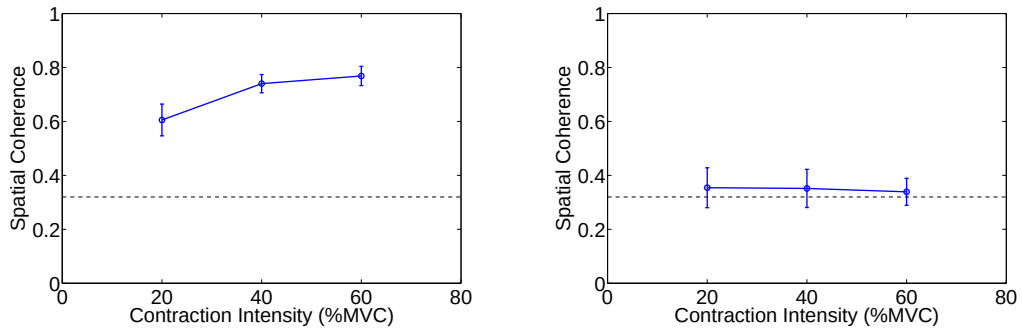

Figure 19: Coherence value averaged in 4 Hz frequency band at f_{MP} for increasing contraction level (a) in longitudinal direction and (b) transverse direction. Error bars indicate one standard deviation over all 10 subjects.

Figure 20 compares the overall spatial coherence value across all trials, subjects, sensor separation distances and contraction level for longitudinal and transverse directions. Using the method of frequency averaged coherence, Fig. 20(a) shows that the spatial coherence value is greater in the longitudinal direction than the transverse direction. Using the mathematically similar method of the normalized cross correlation peak, Fig. 20(b) also shows that the spatial coherence value is greater in the longitudinal direction than the transverse direction.

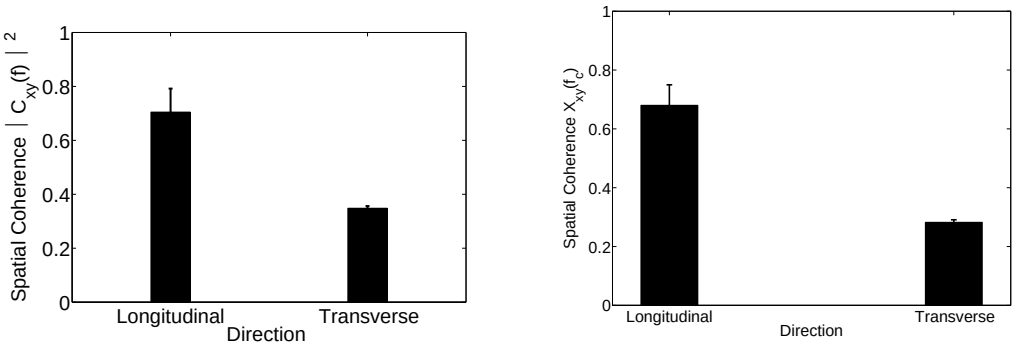

(a) (b)

Figure 20: Overall spatial coherence value across all trials, subjects, sensor separation distances and contraction level for longitudinal and transverse (a) using frequency averaged coherence method averaged in 4 Hz frequency band centered at f_{MP} (b) using normalized cross correlation peak filtered in a 4 Hz frequency band centered at f_{MP}.

CHAPTER V

DISCUSSION

To briefly discuss the quality of measurement taken in this study, the $f_M P$ and signal to noise ratio will be discussed. The results showed that the mean power frequency increased as contraction level increased, which was consistent with results from a previous study that investigated S-MMG mean power frequency using accelerometers on the biceps brachii muscle [33]. In addition, the signal to noise ratio increased as contraction intensity increased, which shows that the experimental setup and protocol enabled good S-MMG signal measurements.

Some supporting findings from this study are that (i) the frequency band at which the S-MMG coherence remains significant is larger for longitudinal sensor pairs than transverse sensor pairs (ii) the S-MMG coherence decreased as sensor separation distance increased (iii) S-MMG coherence increased as the contraction level increased and (iv) the frequency averaged coherence $\mid C_{xy}(f_c) \mid^2$ and the cross correlation peak $X_{xy}(f_c)$ are two separate but comparable ways to determine the directionality of the propagating coherent S-MMG waves. The main finding of this study is that the directionality of propagating coherent S-MMG wave was mainly longitudinal (i.e. along the direction of the biceps brachii muscle fibers).

The initial analysis of the S-MMG data collected for this study confirmed that both the S-MMG mean power frequency and S-MMG signal's intensity increased with the contraction level of the biceps which is in agreement with previously reported findings from studies with similar protocol [46, 47, 33]. The main finding of this study is that the spatial coherence of S-MMG for sensor pairs aligned along the proximal to distal ends of the biceps, (i.e. the longitudinal direction) is significantly higher than

the spatial coherence values for sensor pairs oriented perpendicular to the muscle fiber (i.e. along the transverse direction). Similar results were found when using two related signal processing techniques (namely the magnitude squared coherence function and the maximum of the time-domain cross-correlation function) to estimate the spatial coherence of S-MMG signals filtered in the vicinity of their mean power frequency. In support of the main finding the following three supportive findings were established i) the cut-off frequency of the S-MMG (i.e. the frequency beyond which the spatial coherence values dropped below the confidence level of 0.32 here) is higher for longitudinal sensor pairs (62.38 ± 4.54 Hz) than for transverse sensor pairs (31.70 ± 3.88 Hz) ii) the spatial coherence of S-MMGs along the longitudinal direction decreased with increasing frequency and increasing sensor separation distance and iii) the spatial coherence values between longitudinal sensors pairs increased with contraction level varying between 20% to 60% of the maximum contraction level.

These findings can be related to the physiological origin of S-MMG. First, the local activation of the muscle fibers typically dominates the S-MMG generation mechanism in the higher frequency band (i.e. $f > 25$ Hz) [46]. Furthermore, the fast twitch fibers are more superficially located than slow twitch fibers in the biceps brachii muscle [18]. Hence, in the biceps brachii, the high frequency content of S-MMG, measured with skin-mounted sensors at the biceps brachii surface, is highly influenced by the physical characteristics and orientation of fast twitch fibers, especially at high contraction level [47]. Consequently, the cut-off frequency of the S-MMG (62.38 ± 4.54 Hz) for the longitudinal sensor pairs is likely determined by the highest firing rate of the fast twitch muscles fibers. Second, mechanical vibrations (e.g. as measured by S-MMG) become rapidly attenuated when propagating in viscoelastic materials with high damping factor or viscosity (such as skeletal muscles) [**?**, **?**]. Thus, the propagation distance of such mechanical vibrations is limited by the viscous attenuation and decreases as the frequency content of the vibration increases due to the classical frequency dependence

of the viscous effects [?]. Physically speaking, the S-MMG spatial coherence value indicates the amount of natural muscle vibrations propagating coherently between the two selected sensors. Consequently, the viscous attenuation of the muscle likely limits the sensor separation distance over which S-MMG signals can propagate coherently between the skin-mounted accelerometers, especially as S-MMG frequency increases. Third, as the contraction level increases (between 20% to 60% of the maximum contraction level in this study), the S-MMG generation mechanism is increased due to the recruitment of additional muscle fibers [46, 47], thus resulting the total number of vibration events within the muscle to increase. Furthermore, the muscle's stiffness increases with the contraction level increases [?, ?], thus increasing in turn the mechanical coupling between longitudinal sensor pairs. Consequently, the later two effects likely causes the apparent increase in the spatial coherence values between longitudinal sensors pairs for the tested contraction levels. Finally, the main finding of the paper indicates that the propagation of coherent S-MMG (i.e. propagating between multiple sensors) is highly directional along the muscle longitudinal axis. Indeed the observed longitudinal directionality of the propagating S-MMG along the muscle fiber direction, which is consistent with a previous study [55], is likely determined by the fusiform architectural organization of muscle fibers of the biceps brachii muscle [67] and to some extent the mechanical properties and functionality of the muscle attachments and internal structure of the whole muscle. Consequently measurements of the spatial coherence of high-frequency S-MMG (i.e. $f > 25$ Hz), which are generated by the activity of the muscle fibers) are likely to reflect the physiological architecture of the tested skeletal muscle. Additionally, this may explain why an earlier study of S-MMG coherence of the biceps brachii [52] concluded on a transverse wave propagation of S-MMG (related to a bending transverse modal resonances of the whole biceps) since it was focusing on more energetic lower frequency S-MMG components (i.e. $f < 15$ Hz) which are more affected by motion artifacts (e.g. due

to large movements of the whole limb) and force tremor [9, **?**].

CHAPTER VI

CONCLUSIONS

The variations of the spatial coherence of S-MMG waves across frequency appear to be closely linked to the S-MMG physiological generation mechanism as well as the local elastic properties of the studied muscle. Meaning, the frequency dependency of the coherent S-MMG waves was found to correlate to the physiological basis of muscle force generation. Hence, further studies of the spatial coherence of S-MMG across various muscles could lead to objective measurement techniques of the mechanical properties of skeletal muscles. For different muscles, the same approach can be taken with a few details changed, such as the sensor separation distance and the frequency of interest. Muscles with more slow twitch high endurance muscle fibers would have a lower frequency of interest, if the majority of the force generation is done by the recruitment of these muscle fibers. To this end, the influence of muscular fatigue occurring during voluntary contractions on the spatial coherence of S-MMG requires further quantification. In the study, for the 10 s of data collected there was no clear trend developed that showed the a link between spatial coherence of the S-MMG waves and the length of time of the sub-maximal contraction. Additionally, localization of the strength of coherence in S-MMG between sensor pairs may provide further insights into the potential mechanical compartmentalization that may be due to either localized mechanical properties or localized muscle activity [58] and possible dependency/in-dependency between adjacent muscles or partitions [22, 60, 40]. Finally, S-MMG recorded on single sensor, have typically been used in physiological studies to monitor the mechanical activity of skeletal muscles, in complement to standard surface electromyograms (EMG) which monitor the muscle's electrical activity.

But the characteristics of low-frequency mechanical waves (< 100 Hz here), such as velocity or attenuation, propagating in viscoelastic soft tissues (such as muscle) strongly depend on the local rheological properties of the soft tissues (e.g. compressibility, stiffness) [2]. For instance mechanical waves propagate faster in locally stiffer area [30, 21, 28]. Consequently, S-MMG, which correspond physically to propagating vibrations along the muscle, could allow for passive measurements of the skeletal muscle viscoelastic properties [42, 52, 56, 19] despite the random-looking appearance of the S-MMG time-series.

CHAPTER VII

RECOMMENDATIONS FOR FUTURE WORK

This current work focused on determining the directionality of propagating S-MMG waves by comparing spatial coherence values for sensor pairs in the longitudinal vs transverse directions. This is the first step in determining the viscoelastic properties of skeletal muscle. Now that it has been shown that the S-MMG waves propagate along the longitudinal direction of the biceps brachii muscle, further analysis can be done in determining the speed at which these waves travel. Two methods can be explored to determine the speed at which the S-MMG wave propagates through the muscle. Firstly, using the spatial coherence versus the sensor separation distance data, one can determine a parameter that can describe how the spatial coherence changes versus distance. This would give insight into the propagation speed of the S-MMG waves. Secondly, calculating the cross correlation between two signals in the time domain provides information on the time delay between when the information from the signals are measured at the different location. This can be done by determining the peak of the cross correlation, and time at which that peak occurs. The time where the peak occurs is non-zero for signals that do not have a spatial coherence of 1. This non-zero time value is the time delay between the two signals. Since the distance between the sensors is known, after the time delay between the sensors is found, the propagation velocity can be calculated. Another direction which would prove useful to further expand on the work done here would be to use non-contact to measure S-MMG. Though the accelerometers used were light weight (1 g), there was still a mass loading artifact due to the mass of the accelerometers that may have affected the signal received. Though care was taken to limit the affect of the cables, the cables

may have provided some drag. A non-contact sensor such as a laser vibrometer could be used to measure S-MMG. This would provide a solution to the mass loading and drag artifacts, but would introduce a new challenge. Care must be taken to ensure that the arm stays in the same position. Since the laser is not in physical contact with the arm, the point of measurement can be changed with a slight movement in the arm. With this taken into consideration, using a laser vibrometer could provide useful information with regard to determining viscoelastic properties.

APPENDIX A

MATLAB CODE

A.1 Power Spectrum, MPF, Matrix Plots

```
clear all
tic
for sub=1001:1010
    for per=2:4
        for ifile=1:3
            dirname=['C:\Research\1D_Test\sub',num2str(sub)
                ,'\'];
            %%List the files
            FF=dir(dirname);
            GG={FF.name};GG=GG(3:end);
            kk=1;
            clear data
            LEVEL_TOT=[0 20 40 60];
            count=1;
            ff=0;

            while (count<=length(GG))
                ff=ff+1;
                D=regexp(GG{ff},['sub_',num2str(sub),'_',
                    num2str(LEVEL_TOT(per)),'_',num2str(ifile)
                    ,'.dat']);
```

```
            if length(D)>0
                filename = GG{ff};
            end;
            count=count+1;
        end;

        FPATH=['C:\Research\1D_Test\sub',num2str(sub),'\'];
        fid=fopen([FPATH,filename],'r');
        temp=fread(fid,inf,'double');
        FeORIG=temp(1); %Hz
        num_ch=temp(2); %Number of Channels Recorded

        for idx=1:num_ch
            idx2=idx+2:num_ch:length(temp);
            data(:,idx)=temp(idx2);
        end
        time=1/FeORIG:1/FeORIG:(length(data(:,1)))/FeORIG;
        %save data.mat 'data' 'time' 'freq';
        fclose all; clear fid temp idx idx2 ans;
        %%%%%%%%%%%%%%%%%%%%%%%%%%%%%%%%%%%%%%%%%%%%%%%%%%%%

        timestart=find(time==0.25);
        timeend=find(time==9.75);
        time=time([timestart:timeend]);
```

```
%%%%%%%%%%%%%%%%%%%%%%%%%%%%%%%%%%%%%%%%%%%%%%%%%%%%%%%%%%%%%%%%
data=data([timestart:timeend],:);
data1(:,:)=data(:,[2:17]);
clear data
data=data1;
clear data1
% N=length(time);
% Ts=1/Fe;
% Faxis=[0:N-1]/N/Ts;


%% TO PLOT DATA: UNCOMMENT
dataORIG=data; clear data; %%High sampling rate
RATE=1;
Fe=FeORIG/RATE;Ts=1/Fe;      %Sampling parameters
INIT=0;
%%%%%Decimate to save Memory
for ELT=1:16; %size(dataORIG,2)
    data(:,ELT)=decimate(dataORIG(:,1),RATE);
    dataORIG(:,1)=[];%%Remove line by line to save space

    if INIT==0
        INIT=1;
        %%Define the time axis & frequency axis
        N=length(data);    time=[0:Ts:(N-1)*Ts];
```

```
        freq=[0:1/N/Ts:(N-1)/N/Ts];
        DF=1/N/Ts;% frequency spacing

        %SELECT FREQUENCY BAND
        Fmin1=5; %% Minimum Frequency;
        Fmax1=100; %% Maximum Frequency ;

        %%Define the matlab Filter
        freq_int1=[Fmin1 Fmax1]; [BB1,AA1]=butter(3,[freq_int1]/Fe*2);
    end

    %%%%%%%Filter Data
    data(:,ELT)=filtfilt(BB1,AA1,data(:,ELT));

    %Remove electronic Peak;
    ELEC_PEAK=0;
    if ELEC_PEAK==1
        LABEL_NOTCH='With';
        %%%Remove Electronic Peak centered at 58 Hz and harmonics %%%%%%%%%%%%%%%%%%%%%%%%%%%%%%%%%%%%%%%%%%%%%%%

        for Fcenter=[58, 115] %58*[1 2 3 4]
            freq_intNOTCH=Fcenter+[-1.1 1.1]; [BB,AA]=butter(4,[freq_intNOTCH]/Fe*2,'stop');
```

```
88                          %data(:,ELT)=filtfilt(BB,AA,data(:,
                                ELT));
89                      end
90                      %%%%%%%%%%%%%%%%%%%%%%%%%%%%%%%%
91                  else
92                      LABEL_NOTCH='NO';
93                  end
94
95              end;
96
97
98              %% I remove the last sensor on the tendon
99              Nrem=16;  %Remove 16
100             data(:,Nrem)=[];%%remove last elements
101             clear Fdata;
102             dataORIG=data;
103
104             %% Frequency analysis
105             % Fdata=fft(data,[],1);
106             % Ifreq=find(freq>=Fmin1 & freq<=Fmax1);
107             % MM=max(max(abs(Fdata(Ifreq,:))));
108             % ScaleF=1;
109             % sensor=input('What sensor?');
110             % figure;
111             % plot(freq,abs(Fdata(:,sensor)))
112             % xlim([0  100])
113
```

```
114             %%  Cut the events of high-amplitude
115             THR=median( std(data,[],1))*4;%%Same Threshold
                    for all sensors;
116             TEMP_CLIP_DATA='y' ;%%just filter then
117             %%Equalize data in time domain
118             if TEMP_CLIP_DATA=='y'
119                 for  ELT=1:size(data,2)
120                     II=find(abs(data(:,ELT) )>=THR);%
121                     data(II,ELT)=THR*sign(data(II,ELT) );
122
123                 end
124             end;
125
126             sub=sub-1000;
127
128             %% Compute and plot Power Spectral Desntiy
129
130 %               numseg=40;
131 %               seg=floor(length(data)/numseg);
132 %               segfreq=[0:1/seg/Ts:(seg-1)/seg/Ts];
133 %               a=0;
134 %               while a<(numseg-1)
135 %               F=abs(fft(data(1+a*seg:(a+1)*seg,8)));
136 %                   Fseg(:,a+1)=F;
137 %               a=a+1;
138 %
139 %               end
```

```
140 %               Fseg_tot=mean(Fseg,2);
141 %               figure
142 %               hold on
143 %               plot(segfreq,Fseg_tot)
144 %               xlim([0 100])
145
146
147
148             %% Compute Mean Power Frequency
149             X=freq;
150             Y=abs(fft(data));
151             aaa=find(floor(X)==0); % finds all the indices at
                    which Faxis ~ 0Hz
152             aa=aaa(1); % Index of Faxis = 0Hz
153             bbb=find(floor(X)==100); % finds all the indices
                   at which Faxis ~ 100Hz
154             bb=bbb(1); %% Index of Faxis = 100Hz (100Hz is
                   chosen as the upper bound of frequency range
                   in this case)
155
156             %Calculation of Cut Off Frequency(COF). The COF
                   is defined as the frequency at
157             %which the area under the power spectrum is equal
                    or greater than 90% of
158             %the area for a particular frequency range(0 to
                   100Hz in this case)
159
```

```
160
161             for jj=1:size(Y,2)
162                 totalarea = trapz(X(aa:bb),Y(aa:bb,jj)); %
                        function trapz calculates area under
                        frequency plot from 0 to 100Hz
163                 %using the trapezoidal rule
164                 for ii=1:100  %frequency ranges to be used
                        for calculation (0-100Hz)
165                     xxx=find(floor(X)==ii);
166                     xx=xxx(1);                      %xx = index
                            of Faxis at some frequency ii. The
                            index moves from 0Hz up to the
                            frequency at which 90%
167                     %of the area under the graph has been
                            covered.The value of xx at which 90%
                            of the area is covered
168                     %is the index of Faxis corresponding to
                            the cut-off frequency
169                     area = trapz(X(aa:xx),Y(aa:xx,jj)); %
                            calculates area under graph between 0
                            Hz and the frequency at index xx.
170
171                     if(area >= 0.9*totalarea)
```

```
172                         COF(sub,per,ifile,jj) = X(xx); %this
                                gives the frequency at which the
                                area under the frequency plot is
                                greater or equal to 90% of the
                                total area
173                         break
174                     end
175                 end
176
177                 %mean power frequency
178
179                 M=X(aa:bb);
180                 L=Y(aa:bb,jj);L=L';
181                 MPF(sub,per,ifile,jj) = sum(M.*L)/sum(L); %
                        calculation of mean power frequency(MPF)
182
183             end
184
185
186
187 %% Plot Coherence as Box Plot
188             %  ZZ: coherence  W: frequency bin
189
190             center_freq=mean(MPF(sub,per,ifile,:)); % Average
                    across sensors
191             low_freq=1/3*center_freq;
192             band=4; %Set frequency band for averaging
```

```
193                 cc=1;
194                 for ee=1:size(data,2)
195                     for pos=1:size(data,2)
196                         %Compute avg coherence in the
                                selected freq band
197                         [ZZ,W] =(mscohere(data(:,ee),data(:,
                                pos),[],[],[],Fe));
198                         Iw=find(W>=(center_freq-band/2) & W
                                <=(center_freq+band/2));
199                         Iw1=find(W>=(low_freq-band/2) & W<=(
                                low_freq+band/2));
200 %                       Mcohr(:,pos,ee,per)=ZZ(Iw);
201                         McohrAV_high(sub,ifile,pos,ee,per)=
                                mean(ZZ(Iw));
202                         McohrAV_low(sub,ifile,pos,ee,per)=
                                mean(ZZ(Iw1));
203
204                             %%%%%%%Filter Data
205                             for ELT=1:size(data,2)
206                                 freq_int1=[center_freq-
                                        band/2  center_freq+
                                        band/2];  [BB2,AA2]=
                                        butter(3,[freq_int1]/Fe
                                        *2);
```

```
207                                     freq_int2=[low_freq-band/2
                                            low_freq+band/2];   [
                                        BB3,AA3]=butter(3,[
                                        freq_int2]/Fe*2);
208                                     filtdata_high(:,ELT)=
                                        filtfilt(BB2,AA2,data
                                        (:,ELT));
209                                     filtdata_low(:,ELT)=
                                        filtfilt(BB3,AA3,data
                                        (:,ELT));
210                                 end
211                 %Compute max value of cross correlation in
                        selected freq band
212
213                 CORR_low=xcorr(filtdata_low(:,ee),
                        filtdata_low(:,pos),'coeff');
214                 CORR_high=xcorr(filtdata_high(:,ee),
                        filtdata_high(:,pos),'coeff');
215                         CorrAv_low(sub,ifile,pos,ee,per)=max(
                            CORR_low);
216                         CorrAv_high(sub,ifile,pos,ee,per)=max
                            (CORR_high);
217
218                     end;
219                 end
220                 cohrAV(:,:,per)=CorrAv_high(sub,ifile,:,:,per
                        );
```

```
221      sub=sub+1000;
222              end
223        end
224  end
225
226
227  %% Calculate mean and std of MPF, plot vs MVC
228
229  i=0;
230
231       for sub=1:10
232            for ifile=1:3
233                 for sen=1:15
234  i=i+1;
235  tot_MPF(i,1)=MPF(sub,2,ifile,sen);
236  tot_MPF(i,2)=MPF(sub,3,ifile,sen);
237  tot_MPF(i,3)=MPF(sub,4,ifile,sen);
238                 end
239            end
240       end
241
242  for per=1:3
243       mean_MPF(per)=mean(tot_MPF(:,per));
244       std_MPF(per)=std(tot_MPF(:,per));
245  end
246
247  %
```

```
% for sub=1:10
%     for per=2:4
%         for sen=1:15
%             MPF1(sub,per,sen)=mean(MPF(sub,per,[1:3],sen));
%         end
%     end
% end
% clear MPF
% for sub=1:10
%     for per=2:4
%         MPF(sub,per)=mean(MPF1(sub,per,[1:15]));
%     end
% end
%
% xMPF=[1:15];
 xMVC=[20,40,60];
% figure;
% hold on
% cc=0;
% COLOR_BIG=['b','r','k','m','c','g','y','b','r','k','m','c
    ','g','y','b'];
% for sub=1:10
%     cc=cc+1;
%     plot(xMVC,MPF(sub,[2:4]),COLOR_BIG(cc))
% end
%
% clear MPF1
```

```
274 %
275 % for per=2:4
276 % MPF1(per)=mean(MPF(:,per));
277 % MPFstd(per)=std(MPF(:,per));
278 % end
279 % figure
280 % errorbar(xMVC,MPF1([2:4]),MPFstd([2:4]),'*')
281 % xlim([15 65])
282 % xlabel('% MVC')
283 % ylabel('Mean Power Freq (Hz)')
284 figure;
285  errorbar(xMVC,mean_MPF,std_MPF)
286
287 toc
```

```
 1 clear all
 2 load CorrAV_low.mat
 3 load CorrAV_high.mat
 4 load McohrAV_low.mat
 5 load McohrAV_high.mat
 6 %% Calculate coherence values for distances of 1*delta_x
 7 for sub=1:10
 8     for per=2:4
 9         a=1;
10         for ifile=1:3
11             pos=1;
12             ee=2;
```

```
13              while pos<5
14                  line1(sub,per,1,a)=McohrAV_low(sub,ifile,pos,
                        ee,per);
15                  line1(sub,per,2,a)=McohrAV_high(sub,ifile,pos
                        ,ee,per);
16                  line1(sub,per,3,a)=CorrAv_low(sub,ifile,pos,
                        ee,per);
17                  line1(sub,per,4,a)=CorrAv_high(sub,ifile,pos,
                        ee,per);
18                  pos=pos+1;
19                  ee=ee+1;
20                  a=a+1;
21              end
22              pos=6;
23              ee=7;
24              while pos<10
25                  line1(sub,per,1,a)=McohrAV_low(sub,ifile,pos,
                        ee,per);
26                  line1(sub,per,2,a)=McohrAV_high(sub,ifile,pos
                        ,ee,per);
27                  line1(sub,per,3,a)=CorrAv_low(sub,ifile,pos,
                        ee,per);
28                  line1(sub,per,4,a)=CorrAv_high(sub,ifile,pos,
                        ee,per);
29                  pos=pos+1;
30                  ee=ee+1;
31                  a=a+1;
```

```
32                  end
33                  pos=11;
34                  ee=12;
35                  while pos<15
36                      line1(sub,per,1,a)=McohrAV_low(sub,ifile,pos,
                            ee,per);
37                      line1(sub,per,2,a)=McohrAV_high(sub,ifile,pos
                            ,ee,per);
38                      line1(sub,per,3,a)=CorrAv_low(sub,ifile,pos,
                            ee,per);
39                      line1(sub,per,4,a)=CorrAv_high(sub,ifile,pos,
                            ee,per);
40                      pos=pos+1;
41                      ee=ee+1;
42                      a=a+1;
43                  end
44              end
45          end
46  end
47
48  %% Calculate coherence values for 2*delta_x
49  for sub=1:10
50      for per=2:4
51          a=1;
52          for ifile=1:3
53              pos=1;
54              ee=3;
```

```
55              while pos<4
56                  line2(sub,per,1,a)=McohrAV_low(sub,ifile,pos,
                        ee,per);
57                  line2(sub,per,2,a)=McohrAV_high(sub,ifile,pos
                        ,ee,per);
58                  line2(sub,per,3,a)=CorrAv_low(sub,ifile,pos,
                        ee,per);
59                  line2(sub,per,4,a)=CorrAv_high(sub,ifile,pos,
                        ee,per);
60                  pos=pos+1;
61                  ee=ee+1;
62                  a=a+1;
63              end
64
65              pos=6;
66              ee=8;
67              while pos<9
68
69                  line2(sub,per,1,a)=McohrAV_low(sub,ifile,pos,
                        ee,per);
70                  line2(sub,per,2,a)=McohrAV_high(sub,ifile,pos
                        ,ee,per);
71                  line2(sub,per,3,a)=CorrAv_low(sub,ifile,pos,
                        ee,per);
72                  line2(sub,per,4,a)=CorrAv_high(sub,ifile,pos,
                        ee,per);
73                  pos=pos+1;
```

```
74                      ee=ee+1;
75                      a=a+1;
76                  end
77
78                  pos=11;
79                  ee=13;
80                  while pos<14
81                      line2(sub,per,1,a)=McohrAV_low(sub,ifile,pos,
                            ee,per);
82                      line2(sub,per,2,a)=McohrAV_high(sub,ifile,pos
                            ,ee,per);
83                      line2(sub,per,3,a)=CorrAv_low(sub,ifile,pos,
                            ee,per);
84                      line2(sub,per,4,a)=CorrAv_high(sub,ifile,pos,
                            ee,per);
85                      pos=pos+1;
86                      ee=ee+1;
87                      a=a+1;
88                  end
89              end
90          end
91  end
92
93  %% Calculate coherence values for 3*delta_x
94  for sub=1:10
95      for per=2:4
96          a=1;
```

```
97          for ifile=1:3
98              pos=1;
99              ee=4;
100             while pos<3
101                 line3(sub,per,1,a)=McohrAV_low(sub,ifile,pos,
                        ee,per);
102                 line3(sub,per,2,a)=McohrAV_high(sub,ifile,pos
                        ,ee,per);
103                 line3(sub,per,3,a)=CorrAv_low(sub,ifile,pos,
                        ee,per);
104                 line3(sub,per,4,a)=CorrAv_high(sub,ifile,pos,
                        ee,per);
105                 pos=pos+1;
106                 ee=ee+1;
107                 a=a+1;
108             end
109
110             pos=6;
111             ee=9;
112             while pos<8
113
114                 line3(sub,per,1,a)=McohrAV_low(sub,ifile,pos,
                        ee,per);
115                 line3(sub,per,2,a)=McohrAV_high(sub,ifile,pos
                        ,ee,per);
116                 line3(sub,per,3,a)=CorrAv_low(sub,ifile,pos,
                        ee,per);
```

```
117                     line3(sub,per,4,a)=CorrAv_high(sub,ifile,pos,
                            ee,per);
118                     pos=pos+1;
119                     ee=ee+1;
120                     a=a+1;
121                 end
122
123                 pos=11;
124                 ee=14;
125                 while pos<13
126                     line3(sub,per,1,a)=McohrAV_low(sub,ifile,pos,
                            ee,per);
127                     line3(sub,per,2,a)=McohrAV_high(sub,ifile,pos
                            ,ee,per);
128                     line3(sub,per,3,a)=CorrAv_low(sub,ifile,pos,
                            ee,per);
129                     line3(sub,per,4,a)=CorrAv_high(sub,ifile,pos,
                            ee,per);
130                     pos=pos+1;
131                     ee=ee+1;
132                     a=a+1;
133                 end
134             end
135         end
136 end
137
138
```

```
139 %% Calculate coherence values for 4*delta_x
140 for sub=1:10
141     for per=2:4
142         a=1;
143         for ifile=1:3
144             pos=1;
145             ee=5;
146             line4(sub,per,1,a)=McohrAV_low(sub,ifile,pos,ee,
                    per);
147             line4(sub,per,2,a)=McohrAV_high(sub,ifile,pos,ee,
                    per);
148             line4(sub,per,3,a)=CorrAv_low(sub,ifile,pos,ee,
                    per);
149             line4(sub,per,4,a)=CorrAv_high(sub,ifile,pos,ee,
                    per);
150             a=a+1;
151
152             pos=6;
153             ee=10;
154
155             line4(sub,per,1,a)=McohrAV_low(sub,ifile,pos,ee,
                    per);
156             line4(sub,per,2,a)=McohrAV_high(sub,ifile,pos,ee,
                    per);
157             line4(sub,per,3,a)=CorrAv_low(sub,ifile,pos,ee,
                    per);
```

```
158                 line4(sub,per,4,a)=CorrAv_high(sub,ifile,pos,ee,
                        per);
159                 a=a+1;
160
161
162                 pos=11;
163                 ee=15;
164
165                 line4(sub,per,1,a)=McohrAV_low(sub,ifile,pos,ee,
                        per);
166                 line4(sub,per,2,a)=McohrAV_high(sub,ifile,pos,ee,
                        per);
167                 line4(sub,per,3,a)=CorrAv_low(sub,ifile,pos,ee,
                        per);
168                 line4(sub,per,4,a)=CorrAv_high(sub,ifile,pos,ee,
                        per);
169                 a=a+1;
170
171             end
172         end
173 end
174
175
176 %% Plot Graphs of coherence vs difference for different MVC
177
178
179 for sub=1:10;
```

```
180       for per=2:4;
181           for cond=1:4;
182               y1(sub,per,cond)=mean(line1(sub,per,cond,[25:36])
                      );
183               % y1s=std(line1(sub,per,cond,:));
184               y2(sub,per,cond)=mean(line2(sub,per,cond,[19:27])
                      );
185               % y2s=std(line2(sub,per,cond,:));
186               y3(sub,per,cond)=mean(line3(sub,per,cond,[13:18])
                      );
187               % y3s=std(line3(sub,per,cond,:));
188               y4(sub,per,cond)=mean(line4(sub,per,cond,[7:9]));
189               % y4s=std(line4(sub,per,cond,:));
190           end
191       end
192   end
193
194   for per=2:4
195       for cond=1:4
196           y1_mean(per,cond)=mean(y1(:,per,cond));
197           y1_std(per,cond)=std(y1(:,per,cond));
198           y2_mean(per,cond)=mean(y2(:,per,cond));
199           y2_std(per,cond)=std(y2(:,per,cond));
200           y3_mean(per,cond)=mean(y3(:,per,cond));
201           y3_std(per,cond)=std(y3(:,per,cond));
202           y4_mean(per,cond)=mean(y4(:,per,cond));
203           y4_std(per,cond)=std(y4(:,per,cond));
```

```
204         end
205 end
206
207
208 COLOR_BIG=['b','r','k','m','c','g','y','b','r','k','m','c','g
        ','y'];
209 for cond=1:4
210         figure
211         hold on
212         x=[2 4 6 8 ;1.9 3.9 5.9 7.9 ; 2 4 6 8 ; 2.1 4.1 6.1 8.1];
213         cc=1;
214         for per=2:4
215             y=[y1_mean(per,cond) y2_mean(per,cond) y3_mean(per,
                    cond) y4_mean(per,cond)];
216             ys=[y1_std(per,cond) y2_std(per,cond) y3_std(per,cond
                    ) y4_std(per,cond)];
217             errorbar(x(per,:), y, ys, COLOR_BIG(cc))
218             cc=cc+1;
219         end
220         legend(['20% MVC'],['40% MVC'],['60% MVC'],'Location','
                SouthWest')
221         xlabel('Sensor Separation Distance (cm)')
222         ylim([0 1])
223         if cond==1
224             title(['Coherence Low'])
225         elseif cond==2
226             title(['Coherence High'])
```

```
227     elseif cond==3
228         title(['Correlation Low'])
229     else
230         title(['Correlation High'])
231     end
232 end
233 %\end{verbatim}
```

A.2 Coherence Matrix

```
1  for per=2:4
2      for ifile=1:3
3          for pos=1:15
4              for ee=1:15
5                  cohrAV_high(ifile,pos,ee,per)=mean(
                       McohrAV_high(:,ifile,pos,ee,per));
6                  cohrAV_low(ifile,pos,ee,per)=mean(McohrAV_low
                       (:,ifile,pos,ee,per));
7                  McorrAV_high(ifile,pos,ee,per)=mean(
                       CorrAv_high(:,ifile,pos,ee,per));
8                  McorrAV_low(ifile,pos,ee,per)=mean(CorrAv_low
                       (:,ifile,pos,ee,per));
9              end
10         end
11     end
12 end
13
14 for per=2:4
```

```
15      for pos=1:15
16          for ee=1:15
17              tcohrAV_high(pos,ee,per)=mean(cohrAV_high(:,pos,
                    ee,per));
18              tcohrAV_low(pos,ee,per)=mean(cohrAV_low(:,pos,ee,
                    per));
19              tcorrAV_high(pos,ee,per)=mean(McorrAV_high(:,pos,
                    ee,per));
20              tcorrAV_low(pos,ee,per)=mean(McorrAV_low(:,pos,ee
                    ,per));
21          end
22      end
23  end
24
25  per=3;
26  figure;clf;hold on
27  plot([0.5 0.5],[0 15.5],'-k')
28  cm=colormap(hot);
29  cm1=flipud(cm);
30  colormap(cm1);
31  imagesc(tcohrAV_high(:,:,per),[0.32 1])
32  caxis([0.32,1]);colorbar
33
34  xlabel('Sensor #')
35  ylabel('Sensor #')
36  axis tight
37  axis square
```

```
38 box on
39
40 figure;clf;hold on
41 plot([0.5 0.5],[0 15.5],'-k')
42 cm=colormap(hot);
43 cm1=flipud(cm);
44 colormap(cm1);
45 imagesc(tcohrAV_low(:,:,per),[0.32 1])
46 caxis([0.32,1]);colorbar
47
48 xlabel('Sensor #')
49 ylabel('Sensor #')
50 axis tight
51 axis square
52
53
54 figure;clf;hold on
55 plot([0.5 0.5],[0 15.5],'-k')
56 cm=colormap(hot);
57 cm1=flipud(cm);
58 colormap(cm1);
59 imagesc(tcorrAV_high(:,:,per),[0.32 1])
60 caxis([0.32,1]);colorbar
61
62 xlabel('Sensor #')
63 ylabel('Sensor #')
64 axis tight
```

```
65 axis square
66
67
68 figure;clf;hold on
69 imagesc(tcorrAV_low(:,:,per),[0.32 1])
70 plot([0.5 0.5],[0 15.5],'-k')
71 plot([0.5 15.5],[0.5 0.5],'-k')
72 plot([15.5 15.5],[0.5 15.5],'-k')
73 plot([0.5 15.5],[15.5 15.5],'-k')
74 plot([5.5 5.5],[0.5 15.5],'--k')
75 plot([10.5 10.5],[0.5 15.5],'--k')
76 plot([0.5 15.5],[5.5 5.5],'--k')
77 plot([0.5 15.5],[10.5 10.5],'--k')
78 cm=colormap(hot);
79 cm1=flipud(cm);
80 colormap(cm1);
81 box on
82 caxis([0.32,1]);colorbar
83 h=colorbar;
84 set(h,'fontsize',30);
85
86 % newfilename = regexprep(filename, '_', ' ');
87 % title([newfilename])
88 xlabel('Sensor #')
89 ylabel('Sensor #')
90 axis tight
91 axis square
```

REFERENCES

[1] "The signal processing toolbox ™: Magnitude squared coherence." The Mathworks ™, Oct 2007.

[2] Achenbach, J., *Wave Propagation in Elastic Solids*. Amsterdam, The Netherlands: Elsevier Science Publishers B.V., 1975.

[3] Akataki, K., Mita, K., Itoh, K., Suzuki, N., and Watakabe, M., "Acoustic and electrical activities during voluntary isometric contraction of biceps brachii muscles in patients with spastic cerebral palsy," *MUSCLE & NERVE*, vol. 19, pp. 1252–1257, OCT 1996.

[4] Aki, K., "Space and time spectra of stationary waves, with special reference to microtremors," *Bulletin of the Earthquake Research Institute*, vol. 35, pp. 415–457, 1957.

[5] Allum, J., Dietz, V., and Freund, H., "Neuronal mechanisms underlying physiological tremor," *Journal of Neurophysiology*, vol. 41, no. 3, pp. 557–571, 1978.

[6] Barry, D. and Cole, N., "Muscle sounds are emitted at the resonant frequencies of skeletal muscle," *IEEE Transactions on Biomedical Engineering*, vol. 37, pp. 525–531, May 1990.

[7] Baskin, R. J., "Volume change and pressure development in muscle during contraction," *American Journal of Physiology*, vol. 213, pp. 1025–1030, 1967.

[8] Beck, T. W., Housh, T. J., Cramer, J. T., Weir, J. P., Johnson, G. O., Coburn, J. W., Malek, M. H., and Mielke, M., "Mechanomyographic amplitude and frequency responses during dynamic muscle actions: a comprehensive review.," *Biomedical Engineering Online*, vol. 4, pp. 1–27, 2005.

[9] Brown, T., Rack, P., and Ross, H., "Different types of tremor in the human thumb," *Journal of Physiology-London*, vol. 332, no. Nov, pp. 113–123, 1982.

[10] Brunetti, F., Rocon, E., Pons, J., and Manto, M., "The tremor coherence analyzer (tca): A portbale tool to asses instantaneous inter-muscle coupling in tremor," in *Proceedings of the 26th Annual International Conference of the IEEE EMBS*, pp. 61–64, 2004.

[11] Carter, G., "Coherence and time-delay estimation," *Proceedings of the IEEE*, vol. 75, pp. 236–255, Feb 1987.

[12] Cescon, C., Farina, D., Gobbo, M., Merletti, R., and Orizio, C., "Effect of accelerometer location on mechanomyogram variables during voluntary, constant-force contractions in three human muscles," *Medical & Biological Engineering & Computing*, vol. 42, pp. 121–127, Jan 2004.

[13] Cescon, C., Madeleine, P., and Farina, D., "Longitudinal and transverse propagation of surface mechanomyographic waves generated by single motor unit activity," *Medical & Biological Engineering & Computing*, vol. 46, pp. 871–877, Sep 2008.

[14] Cescon, C., Madeleine, P., Graven-Nielsen, T., Merletti, R., and Farina, D., "Two-dimensional spatial distribution of surface mechanomyographical response to single motor unit activity," *Journal of Neuroscience Methods*, vol. 159, pp. 19–25, Jan 2007.

[15] Challis, R. and Kitney, R., "Biomedical signal-processing 3. the power spectrum and coherence function," *Medical & Biological Engineering & Computing*, vol. 29, pp. 225–241, May 1991.

[16] Chen, D., Durand, L., and Bellemare, F., "Time and frequency domain analysis of acoustic signals from a human muscle," *MUSCLE & NERVE*, vol. 20, pp. 991–1001, AUG 1997.

[17] Chen, S., Fatemi, M., and Greenleaf, J. F., "Quantifying elasticity and viscosity from measurement of shear wave speed dispersion," *The Journal of the Acoustical Society of America*, vol. 115, no. 6, pp. 2781–2785, 2004.

[18] Clamann, H., "Activity of single motor units during isometric tension," *Neurology*, vol. 20, no. 3, pp. 254–260, 1970.

[19] Cole, N. and Barry, D., "Muscle sounds frequencies of the frog are modulcated by Skeletal-muscle tension," *Biophysical Journal*, vol. 66, pp. 1104–1114, Apr 1994.

[20] Cox, H., "Spatial correlation in arbitrary noise fields with application to ambient sea noise," *Journal of the Acoustical Society of America*, vol. 54, no. 5, pp. 1289–1301, 1973.

[21] Dresner, M., Rose, G., Rossman, P., Muthupillai, R., Manduca, A., and Ehman, R., "Magnetic resonance elastography of skeletal muscle," *Journal of Magnetic Resonance Imaging*, vol. 13, pp. 269–276, Feb 2001.

[22] English, A., Wolf, S., and Segal, R., "Compartmentalization of Muscles and Their Motor Nuclei - The Partitioning Hypothesis," *Physical Therapy*, vol. 73, pp. 857–867, Dec 1993.

[23] Esposito, F., Malgrati, D., Veicsteinas, A., and Orizio, C., "Time and frequency domain analysis of electromyogram and sound myogram in the

elderly," *EUROPEAN JOURNAL OF APPLIED PHYSIOLOGY AND OCCUPATIONAL PHYSIOLOGY*, vol. 73, pp. 503–510, JUL 1996.

[24] Farina, D., Li, X., and Madeleine, P., "Motor unit acceleration maps and interference mechanomyographic distribution," *Journal of Biomechanics*, vol. 41, pp. 2843–2849, Sep 2008.

[25] Freund, H., "Motor unit and muscle-activity in voluntary motor control," *Physiological Reviews*, vol. 63, no. 2, pp. 387–436, 1983.

[26] Gardner, W. A., "A unifying view of coherence in signal processing," *Signal Processing*, vol. 29, no. 2, pp. 113 – 140, 1992.

[27] Gennisson, J., Baldeweck, T., Tanter, M., Catheline, S., Fink, M., Sandrin, L., Cornillon, C., and Querleux, B., "Assessment of elastic parameters of human skin using dynamic elastography," *IEEE Transactions on Ultrasonics Ferroelectrics and Frequency Control*, vol. 51, pp. 980–989, Aug 2004.

[28] Gennisson, J., Catheline, S., Chaffai, S., and Fink, M., "Transient elastography in anisotropic medium: Application to the measurement of slow and fast shear wave speeds in muscles," *Journal of the Acoustical Society of America*, vol. 114, pp. 536–541, Jul 2003.

[29] Graaff, K. V. D., *Human Anatomy*. New York, New York: McGraw-Hill, 6 ed., 2002.

[30] Greenleaf, J., Fatemi, M., and Insana, M., "Selected methods for imaging elastic properties of biological tissues," *Annual Review of Biomedical Engineering*, vol. 5, pp. 57–78, 2003.

[31] Halliday, D., Rosenberg, J., Amjad, A., Breeze, P., Conway, B., and Farmer, S., "A framework for the analysis of mixed time series/point process data - theory and application to the study of physiological tremor, single motor unit discharges and electromyograms," *Progress in Biophysics & Molecular Biology*, vol. 64, no. 2-3, pp. 237–278, 1995.

[32] Huxley, H. E., "The mechanism of muscular contraction," *Science*, vol. 164, no. 3886, pp. 1356–1366, 1969.

[33] Jasklska, A., Madeleine, P., Jasklski, A., Kisiel-Sajewicz, K., and Arendt-Nielsen, L., "A comparison between mechanomyographic condenser microphone and accelerometer measurements during submaximal isometric, concentric and eccentric contractions," *Journal of Electromyography and Kinesiology*, vol. 17, no. 3, pp. 336 – 347, 2007.

[34] Kim, T., Shimomura, Y., Iwanaga, K., and Katsuura, T., "Comparison of an accelerometer and a condenser microphone for mechanomyographic signals during measurement of agonist and antagonist muscles in sustained isometric

muscle contractions.," *Journal of Physiology and Anthropolgy*, vol. 27, pp. 121–131, 2008.

[35] Kim, T., Shimomura, Y., Iwanaga, K., and Katsuura, T., "Influence of force tremor on mechanomyographic signals recorded with an accelerometer and a condenser microphone during measurement of agonist and antagonist muscles in voluntary submaximal isometric contractions.," *Journal of Physiology and Anthropolgy*, vol. 27, pp. 33–42, 2008.

[36] Kimura, T., Hamada, T., Watanabe, T., Maeda, A., Oya, T., and Moritani, T., "Mechanomyographic responses in human biceps brachii and soleus during sustained isometric contraction," *European Journal of Applied Physiology*, vol. 92, pp. 533–539, Aug 2004.

[37] Kwatny, E., Thomas, D. H., and Kwatny, H. G., "An application of signal processing techniques to the study of myoelectric signals," *IEEE Transactions on Biomedical Engineering*, vol. 17, pp. 303–313, 1970.

[38] Larose, E., Roux, P., and Campillo, M., "Reconstruction of Rayleigh-Lamb dispersion spectrum based on noise obtained from an air-jet forcing," *JOURNAL OF THE ACOUSTICAL SOCIETY OF AMERICA*, vol. 122, pp. 3437–3444, DEC 2007.

[39] Lieber, R., Steinman, S., Barash, I., and Chambers, H., "Structural and functional changes in spastic skeletal muscle," *MUSCLE & NERVE*, vol. 29, pp. 615–627, MAY 2004.

[40] M Shinohara, Y. Y. and Kouzaki, M., "Alterations in synergistic muscle activation impact fluctuations in net force," *Medicine and Science in Sports and Exercise, in press*, 2008.

[41] Madeleine, P., Farina, D., Merletti, R., and Arendt-Nielsen, L., "Upper trapezius muscle mechanomyographic and electromyographic activity in humans during low force fatiguing and non-fatiguing contractions," *European Journal of Applied Physiology*, vol. 87, pp. 327–336, Aug 2002.

[42] Madeleine, P., Cescon, C., and Farina, D., "Spatial and force dependency of mechanomyographic signal features," *Journal of Neuroscience Methods*, vol. 158, pp. 89–99, Nov 2006.

[43] Madeleine, P., Tuker, K., Arendt-Nielsen, L., and Farina, D., "Heterogeneous mechanomyographic absolute activation of paraspinal muscles assessed by a two-dimensional array during short and sustained contractions," *Journal of Biomechanics*, vol. 40, no. 12, pp. 2663–2671, 2007.

[44] Malhotra, S., Cousins, E., Ward, A., Day, C., Jones, P., Roffe, C., and Pandyan, A., "An investigation into the agreement between clinical, biomechanical and neurophysiological measures of spasticity," *CLINICAL REHABILITATION*, vol. 22, no. 12, pp. 1105–1115, 2008.

[45] Mason, P., "Dynamic stiffness and crossbridge action in muscle," *Biophysics of Structure & Mechanism*, vol. 4, pp. 15–25, 1977.

[46] Orizio, C., "Muscle sound - bases for the introduction of a mechanomyogram signal in muscle studies," *Critical Reviews in Biomedical Engineering*, vol. 21, no. 3, pp. 201–243, 1993.

[47] Orizio, C., *Surface Mechanomyogram (Chapter 11 of Electromyography)*. Wiley-IEEE Press, 2005.

[48] Orizio, C., Gobbo, M., Diemont, B., Esposito, F., and Veicsteinas, A., "The surface mechanomyogram as a tool to describe the influence of fatigue on biceps brachii motor unit activation strategy. Historical basis and novel evidence," *EUROPEAN JOURNAL OF APPLIED PHYSIOLOGY*, vol. 90, pp. 326–336, OCT 2003.

[49] Orizio, C., Liberati, D., Locatelli, C., DeGrandis, D., and Veicsteinas, A., "Surface mechanomyogram reflects muscle fibres twitches summation," *Journal of Biomechanics*, vol. 29, pp. 475–481, Apr 1996.

[50] ORIZIO, C. and VEICSTEINAS, A., "SOUNDMYOGRAM ANALYSIS DURING SUSTAINED MAXIMAL VOLUNTARY CONTRACTION IN SPRINTERS AND LONG-DISTANCE RUNNERS," *INTERNATIONAL JOURNAL OF SPORTS MEDICINE*, vol. 13, pp. 594–599, NOV 1992.

[51] Oster, G. and Jaffe, J., "Low-frequency sounds from sustained contraction of human skeletal-muscle," *Biophysical Journal*, vol. 30, no. 1, pp. 119–127, 1980.

[52] Ouamer, M., Boiteux, M., Petitjean, M., Travens, L., and Sales, A., "Acoustic myography during voluntary isometric contraction reveals non-propagative lateral vibration," *Journal of Biomechanics*, vol. 32, pp. 1279–1285, Dec 1999.

[53] Pappas, G., Asakawa, D., Delp, S., Zajac, F., and Drace, J., "Nonuniform shortening in the biceps brachii during elbow flexion," *Journal of Applied Physiology*, vol. 92, pp. 2381–2389, Jun 2002.

[54] Prochazka, A. and Trend, P., "Instability in human forearm movements studied with feed-back-controlled muscle vibration," *Journal of Physiology-London*, vol. 402, pp. 421–442, Aug 1988.

[55] Sabra, K. G. and Archer, A., "Tomographic elastography of contracting skeletal muscles from their natural vibrations," *Applied Physics Letters*, vol. 95, NOV 16 2009.

[56] Sabra, K. G., Conti, S., Roux, P., and Kuperman, W. A., "Passive in vivo elastography from skeletal muscle noise," *Applied Physics Letters*, vol. 90, May 2007.

[57] Sabra, K., Roux, P., and Kuperman, W., "Emergence rate of the time-domain Green's function from the ambient noise cross-correlation function," *JOURNAL OF THE ACOUSTICAL SOCIETY OF AMERICA*, vol. 118, pp. 3524–3531, DEC 2005.

[58] Segal, R., "Neuromuscular compartments in the human biceps brachii muscle," *Neuroscience Letters*, vol. 140, pp. 98–102, Jun 8 1992.

[59] Shapiro, N., Campillo, M., Stehly, L., and Ritzwoller, M., "High-resolution surface-wave tomography from ambient seismic noise," *SCIENCE*, vol. 307, pp. 1615–1618, MAR 11 2005.

[60] Shinohara, M., "Muscle activation strategies in multiple muscle systems," *Medicine and Science in Sports and Exercise, in press*, 2008.

[61] Shinohara, M., Kouzaki, M., Yoshihisa, T., and Fukunaga, T., "Mechanomyography of the human quadriceps muscle during incremental cycle ergometry," *European Journal of Applied Physiology and Occupational Physiology*, vol. 76, pp. 314–319, Oct 1997.

[62] Shinohara, M., Kouzaki, M., Yoshihisa, T., and Fukunaga, T., "Mechanomyogram from the different heads of the quadriceps muscle during incremental knee extension," *European Journal of Applied Physiology*, vol. 78, pp. 289–295, Sep 1998.

[63] Shinohara, M. and Sogaard, K., "Mechanomyography for studying force fluctuations and muscle fatigue," *Exercise and Sport Science Reviews*, vol. 34, pp. 59–64, Apr 2006.

[64] Tarata, M. T., "Mechanomyography versus electromyography, in monitoring the muscular fatigue," *Biomedical Engineering Online*, vol. 2, 2003.

[65] Wakatabe, M., Mita, K., Akataki, K., and Ito, K., "Reliability of the mechanomyogram detected with an accelerometer during voluntary contracts," *Medical & Biological Engineering & Computing*, vol. 41, pp. 198–202, 2003.

[66] Weaver, R. and Lobkis, O., "Ultrasonics without a source: Thermal fluctuation correlations at MHz frequencies," *PHYSICAL REVIEW LETTERS*, vol. 87, SEP 24 2001.

[67] Winter, D. A., *Biomechanics and Motor Control of Human Movement*. New York, New York: John Wiley & Sons, 1990.

[68] Yoshitake, Y., Shinohara, M., Ue, H., and Moritani, T., "Characteristics of surface mechanomyogram are dependent on development of fusion of motor units in humans," *Journal of Applied Physiology*, vol. 93, pp. 1744–1752, Nov 2002.

[69] Yoshitake, Y., Masani, K., and Shinohara, M., "Laser-detected lateral muscle displacement is correlated with force fluctuations during voluntary contractions in humans," *Journal of Neuroscience Methods*, vol. 173, pp. 271–278, Aug 2008.